TRIUMF

ANNUAL REPORT
SCIENTIFIC ACTIVITIES

2001

NUCLEAR AND ATOMIC PHYSICS

Experiment 704
Charge symmetry breaking in $np \to d\pi^0$ close to threshold
(A.K. Opper, Ohio; E. Korkmaz, UNBC)

Experiment 704 expects to have final results from its high precision measurement of charge symmetry breaking in the strong interaction completed by mid-2002. The observable of interest is the forward-backward asymmetry (A_{fb}) in $np \to d\pi^0$, which must be zero in the centre of mass if charge symmetry is conserved and has a predicted value that ranges between $(-35 \to +70) \times 10^{-4}$ [Niskanen, Few-Body Systems **26**, 241 (1999); van Kolck *et al.*, Phys. Lett. **B493**, 65 (2000)] depending on the strengths of the various contributions. The forward-backward asymmetry is defined as

$$A_{fb}(\theta) \equiv \frac{\sigma(\theta) - \sigma(\pi - \theta)}{\sigma(\theta) + \sigma(\pi - \theta)}$$

with the relevant contributions being the neutron-proton mass difference (δ), exchange of an isospin mixed $\eta - \pi$ meson, and the effect of the $d\ u$ quark mass difference on pion nucleon scattering.

The experiment was carried out with a 279.5 MeV neutron beam, a liquid hydrogen target, and the SASP spectrometer positioned at $0°$. With these kinematics, and the large acceptance of SASP, the full deuteron distribution was detected in one setting of the spectrometer, thereby eliminating many systematic uncertainties. Measurements of np elastic scattering with incident neutron beams that fill the same target space and produce protons that span the momentum distribution of the $np \to d\pi^0$ reaction provide a stringent test of the acceptance description of the spectrometer. With over seven million $np \to d\pi^0$ events and six million np elastic events, the statistical uncertainty of this measurement is 5×10^{-4}. The anticipated systematic uncertainty is 7×10^{-4}, as indicated in Fig. 33.

Data analysis

Experiment 704 production data were analyzed in four successive passes: (1) detector calibration; (2) beam direction determination in the SASP-centric front end wire chamber coordinate system; (3) final extraction of the deuteron kinematic locus (see Fig. 34); and (4) efficiency determination. In addition to extracting the kinematic locus and detector efficiencies, the last pass of analysis also produced a filtered data set of 8 words/event (four target variables and four focal plane variables) for all good locus events. The filtered data set of $\sim$200 Mbytes can be resorted and analyzed in one hour on a Linux box. The final
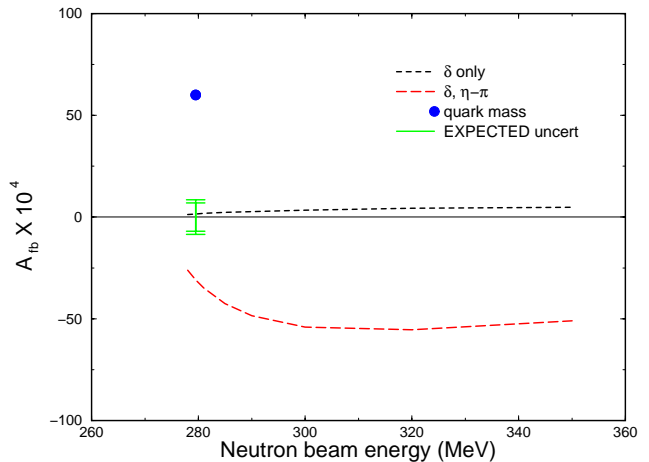
Integrated A$_{fb}$ for different neutron lab energies

Fig. 33. Calculated contributions to A_{fb} and *anticipated* uncertainties.
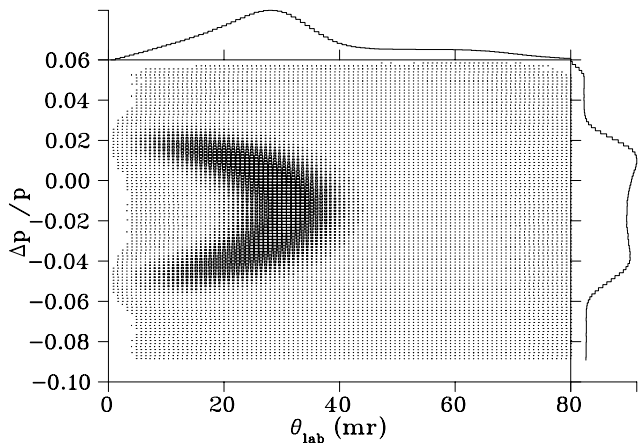
Fig. 34. Kinematic locus of all $np \to d\pi^0$ data.

analysis of the $np \to d\pi^0$ data took approximately two months and was finished at the end of September, 2000.

Extraction of A_{fb}

The data have the accumulated effects of multiple scattering, energy loss, and other physical processes which make extracting A_{fb} directly from the locus impossible. As such, Monte Carlo techniques are used to extract the angle integrated A_{fb}. Close to threshold the $np \to d\pi^0$ cross section in the centre of mass frame is given by:

$$\frac{d\sigma}{d\Omega} = A_0 + A_1 P_1(\cos(\theta)) + A_2 P_2(\cos(\theta)),$$

where P_i are Legendre polynomials, θ is the centre of mass scattering angle [Hutcheon *et al.*, Nucl. Phys. **A535**, 618 (1991)]. The presence of charge symmetry

38

breaking will be reflected in the A_1 term as it is odd in terms of $\cos\theta$. The angle integrated form of A_{fb} is given by

$$A_{fb} = \frac{1}{2}A_1/A_0.$$

Thus, determining the value of A_1, which minimizes the χ^2 of the fit between the real and simulated data, determines A_{fb}.

Due to the strong sensitivity of A_{fb} to the central momentum of the spectrometer (p_0), the LH$_2$ target thickness, and the average energy of the primary beam (T_{beam}), the simulation must span a four dimensional space defined by these three experimental parameters and A_1/A_0. This procedure requires generating simulations at the nominal values, plus a canonical step, and minus a canonical step for each parameter. With a four dimensional parameter space needing to be covered, this means 81 (i.e. 3^4) independent simulations must be generated. The comparison of data to these simulations produces a four dimensional χ^2 space and the values of the four parameters that give a global minimum of that χ^2 space determine the value of A_1/A_0 and consequently A_{fb}.

Simulation

The simulation is based on GEANT and begins with a proton beam incident on a ^{7}Li target to reproduce the energy loss effects in that target. The model of the equipment is in agreement with the best known blueprints, "as-built drawings", and recent measurements. The SASP dipole field used in the simulation is a map of that magnet at 875 A, scaled up to the running current of 905 A. Data were acquired in 19 different periods spanning two years and the simulation "schedules in" measured detector efficiencies, scintillator thresholds, and missing wires in a manner consistent with the actual running periods. The simulation also allows the target thickness and average beam energy to vary for each of the data-taking periods.

To reduce the possibility of psychological bias in matching simulation to data, a "black box" subroutine has been added to the simulation. This routine adds a (hidden) offset to the A_1/A_0 asymmetry parameter used to set up the $np \rightarrow d\pi^0$ generator in the simulation. After selecting the value for the offset, a member of the collaboration not involved in simulation development compiled the subroutine on all simulation farms, mailed the source code to two people outside the collaboration, and deleted the source code.

Hadronic losses

Deuteron reaction losses, which account for 1–2% of all deuteron events, have a significant momentum

dependence over the 8% momentum range of the experiment. Reactions on carbon are the dominant processes and include significant contributions from both elastic and reaction processes. Including these processes in the simulation required that these processes be parametrized from the world's data on deuteron elastic and reaction cross sections from hydrogen and carbon [Auce *et al.*, Phys. Rev. **C53**, 2919 (1996); Saturne, Nucl. Phys. **A464**, 717 (1987); Okamura *et al.*, Phys. Rev. **C58**, 2180 (1998); Baumer *et al.*, Phys. Rev. **C63**, 037601 (2001)]. As such, the systematic uncertainty in A_{fb} associated with the deuteron hadronic losses is a function of the uncertainties in the world's data. Due to complexities in the simulation, the systematic uncertainty in A_{fb} associated with the deuteron hadronic losses could not easily be deduced directly from the parametrization of the deuteron hadronic processes in the simulation. Instead, an estimate of the false asymmetry introduced by deuteron hadronic processes was obtained by comparing the change in simulation output with the hadronic processes being turned on and off. The ratio of these outputs is referred to as R and is a function of the deuteron momentum. Assuming a simple relationship for the momentum dependence of the hadronic processes, a linear function:

$$R(\delta) = a + b\delta$$

is fit to the ratio with $a = 0.9365 \pm 0.005$ and $b = 0.13 \pm 0.02$. With the exclusion of deuteron hadronic losses, it is assumed that the deuteron locus is spread over a momentum interval of (2Δ) for which the count density (C) is constant.

Incorporating hadronic processes into the reaction should produce a count density (C') which is proportional to the change in count ratio:

$$C' = C(a + b\delta).$$

Integrating C' from $-\Delta$ to 0 (0 to Δ) gives the number of backward (forward) going deuterons and inserting these into A_{fb} gives the change in A_{fb} as:

$$A_{fb} = \frac{b\Delta}{2a}.$$

Using the values found for a and b, the false asymmetry introduced by the energy dependence in the total cross section was found to be 0.28% when comparing reaction losses on and off in the simulation. With the uncertainty in the energy dependence of the cross section being approximately 30 mb in 539 mb, the systematic uncertainty in A_{fb} is in the order of 0.016%.

Model of SASP acceptance

The acceptance of SASP is a complicated function of the position and angle at which the deuteron is produced and its momentum (X_i, θ_i, Y_i, ϕ_i, and δ). Describing this acceptance properly requires an accurate model of the magnetic fields in SASP because (1) deuterons can collide with interior surfaces of SASP and be lost from the locus, and (2) the reconstructed momentum variable, which is a function of the focal plane variables X_f and θ_f, may be distorted in a momentum dependent way by an inaccurate model.

The np elastic scattering data provide the best means to determine the acceptance in that the incident beam of this reaction fills the target parameter space in a way that is similar to that of the $np \to d\pi^0$ reaction. To investigate momentum dependent effects, projections of Y_i and ϕ_i have been made for slices in X_i and θ_i and ratios of these distributions made for data vs. GEANT and for the –4% vs. +4% momentum sets. The basic features of these ratios are understood in terms of the focusing action of the SASP entrance quads, Q1 and Q2. These features appear in both data and GEANT, but GEANT does not accurately represent the shoulder region where the acceptance in ϕ_i begins to fall. Consequently, we have determined cuts which exclude those portions of the acceptance that cannot be adequately modelled. These cuts are on target position and angle and define regions of uniform acceptance. Much effort was directed at developing a method to find the flat acceptance range in an automated and unbiased manner.

Systematic uncertainties and error budget

Simulation vs. simulation comparisons were carried out to determine how strongly the experimental parameters are correlated with A_1/A_0. For each parameter this involved simulating kinematic locus scatter plots for a 3×3 grid of the experimental parameter vs. A_1/A_0, calculating the χ^2 of those nine plots when compared to a plot simulated with nominal values, and fitting the χ^2 space. The correlation of A_1/A_0 with the experimental parameter was then obtained from the error matrix based on the curvature of the χ^2 space. Combining this correlation with the uncertainty in the parameter gives the systematic uncertainty of A_1/A_0 due to that experimental parameter. Note that the uncertainty in the parameter comes from a separate determination and not from the χ^2 minimization.

These studies quantified the expected strong sensitivity of A_1/A_0 to p_0, the LH$_2$ target thickness, and T_{beam}. The only way to reduce the systematic effects of these parameters on A_1/A_0 is to reduce the uncertainties of these parameters. This was done by letting these three parameters and A_1/A_0 vary freely and determining the values which minimize the χ^2 of the fit between data and the simulation. With the whole kinematic locus constraining the fit, the uncertainties in the parameters were greatly reduced. As mentioned above, this procedure required generating simulations at three different values for each parameter. The curvature of the resulting 4D χ^2 space gave the set of sensitivities and uncertainties shown in Table IV.

Table IV. Systematic uncertainties from the main grid.

Parameter	Sensitivity	Uncertainty	$\Delta A_1/A_0$
p_0	42.9%/%	±0.0015%	0.066%
LH$_2$	1.2%/mm	±0.043 mm	0.052%
T_{beam}	-7.22%/MeV	±0.0012 MeV	-0.0087%

The systematic uncertainty in A_1/A_0 resulting from adding the above uncertainties in quadrature is 8.5×10^{-4}; this yields a systematic uncertainty in A_{fb} of 4.3×10^{-4}. The overall error budget, based on simulation vs. simulation studies and the 4D parameter space is given in Table V.

Table V. Error budget.

	Uncertainty A_{fb} (10^{-4})
FEV threshold	2.5
FEC separation	2.5
Li target position	2.5
A_2/A_0	2
Deuteron losses	1.5
Efficiencies	1.5
$\sigma(T)$	1
Neutron angle	1
Background	1
FET threshold	0.5
Fit	4.3
Total systematics	7.1
Statistics	5
Total uncertainty	9

Verification of acceptance model

The np elastic scattering data have been used to determine the regions of target space and angle which yield a flat acceptance for the SASP spectrometer. As mentioned above, this reaction is the best way to identify these regions as the incident beam of this reaction fills the target parameter space in a way that is similar to that of the $np \to d\pi^0$ reaction. In a robust test of the uniformity of the acceptance, A_1/A_0 was extracted for various subsets of the target space.

Table VI. Stability of A_1/A_0 for target subspaces; first simulation set.

$X_i \ Y_i$	Angular	$\Delta(A_1/A_0)$ (10^{-4})
standard $\pm$ 2 cm	standard	0
standard	8 mr tighter	2 ± 14
$r <$ 2 cm	standard	-6.5 ± 14
$r <$ 1 cm	standard	-22.7 ± 24
± 1 cm	standard	-23.4 ± 21
± 0.66 cm	standard	2.6 ± 32
standard	ϕ_1	34.6 ± 27
standard	ϕ_2	32.6 ± 23
standard	ϕ_3	-44.4 ± 38
standard	ϕ_4	-28.4 ± 24
bottom	standard	-102.2 ± 19
top	standard	83.7 ± 18
left	standard	5.6 ± 19
right	standard	-16.7 ± 18

Table VII. Stability of the four free parameters for target subspaces; second simulation set.

	$\Delta(A_1/A_0)$ (10^{-4})	LH$_2$ (mm)	p_0 (MeV/c)	T_{beam} (MeV)
std	0 ± 14	0.72 ± 0.05	0.425 ± 0.013	0.072 ± 0.001
b	-9 ± 20	0.35 ± 0.07	0.645 ± 0.019	0.118 ± 0.002
t	2 ± 19	1.02 ± 0.07	0.237 ± 0.018	0.031 ± 0.002
l	-5 ± 20	0.74 ± 0.07	0.343 ± 0.019	0.068 ± 0.002
r	2 ± 19	0.72 ± 0.07	0.496 ± 0.018	0.075 ± 0.002

std = standard; b = bottom; t = top; l = left; r = right

inconsistency of the other parameters of the fit suggests that a feature of the acceptance is still not understood.

Final steps

In looking for the problem with the acceptance, another inconsistency between the simulation description of the FET scintillators and the true scintillators was discovered. The gap between the upper and lower halves of the FET was centred at $X_i = 0.152$ cm, but was positioned in the simulation at $X_i = -0.173$ cm. This mismatch yielded a region 0.325 cm high in which the energy loss in the FET was not calculated correctly by the simulation. The mismatch has been corrected and the agreement in simulation and data gap positions can be seen in Fig. 35.

It is unlikely that the gap mismatch alone could cause the inconsistencies seen in p_0, LH$_2$ thickness, and T_{beam} for the different acceptance subspaces. Before investing the cpu time to generate a new set of simulations with the corrected gap position, we are working to eliminate any other systematic effects.
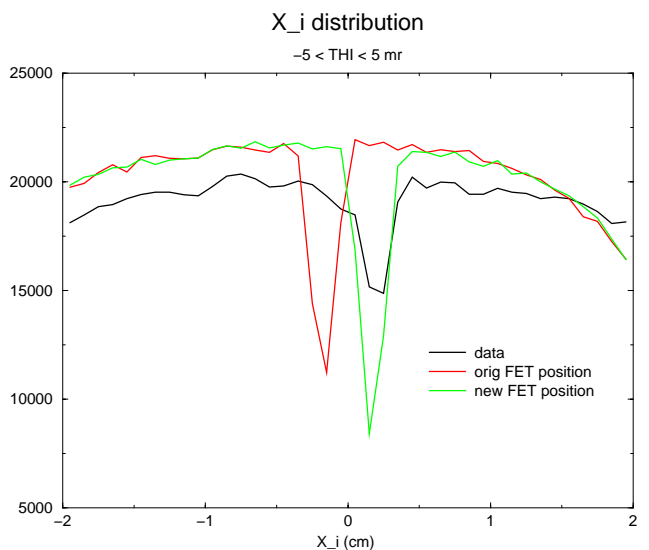
Initially the results of this study, shown in Table VI, indicated that the extracted value of A_1/A_0 is stable over the acceptance subspaces. However, the last set of subspaces to be analyzed uncovered a surprising difference in A_1/A_0 for the top and bottom subspaces. The source of this discrepancy was an inconsistency between the front end trigger scintillator (FET) thicknesses used in the simulation and their true thicknesses. The FET is a pair of scintillators, one above the other, to reduce sagging of the PMTs when exposed to the high rates of this experiment, ~ 5 MHz. A major project undertaken in 2000 was the verification of the description of the equipment in the simulation; this involved remeasuring much of the equipment. Logbook entries from that project give the top scintillator thickness as 0.159 cm and that of the bottom scintillator as 0.170 cm. The simulation naively used the average of these, which meant that the energy loss of the deuterons as they passed through the FET scintillators was incorrect. With the strong sensitivity of A_1/A_0 to energy (see Table IV), a false A_{fb} was systematically introduced into the simulation.

After correcting the FET scintillator thicknesses, a new set of 81 simulations was generated covering the 4D parameter space. Generating a new set of simulations requires 1100 cpu-days on a Linux box. When done on the four Linux clusters available to us, this takes about four weeks of live time. This new set of simulations showed much better agreement of A_1/A_0 for the different acceptance subspaces, however, the values of the other three parameters at the global minimum were not stable for the top and bottom halves of the acceptance (see Table VII). While the different acceptance subspaces give consistent values of A_1/A_0, the

Fig. 35. X_i position of FET gap; -5 mr $< \phi_i < 5$ mr.

Experiment 715
Weak interaction symmetries in β^+ decay of optically trapped ^{37,38m}K

(J.A. Behr, TRIUMF; K.P. Jackson, TRIUMF/SFU)

The experimental progress of the TRIUMF neutral atom trap program in the last year will all be summarized in this section of the Annual Report.

Data taken in fall, 2000 for the β^+-ν correlation measurement in the $0^+ \rightarrow 0^+$ pure Fermi decay of ^{38m}K are still under analysis. From these data, limits have been set on the admixture of possible heavy (0.7–3.8 MeV) neutrinos with the electron neutrino, producing a Ph.D. thesis and an imminent publication. The status of these experiments will be briefly summarized here.

The spin-polarized program has completed analysis of the test ^{37}K data taken in November, 2000. In the off-line lab, nuclear vector polarization of stable ^{41}K has now reached sufficient quality to schedule a test run right-handed current search in ^{37}K in the next running period. A possible polarization systematic, a subtle atomic physics effect called "coherent population trapping", has been identified and eliminated. Its careful characterization is now being prepared for publication, and explored as a possible spectroscopy technique on the radioactives.

The December, 2001 EEC approved two new shorter-term experiments which will also be summarized here. Experiment 925, isospin mixing in ^{36}Ar via spin-polarized observable in ^{36}K β^+ decay, will test the nuclear structure calculations needed to extract V_{ud} from Fermi strength data. Experiment 926, measurement of charge radius and β^+ decay Q-value of laser-trapped ^{74}Rb, will also produce a small contribution to the understanding of V_{ud}.

^{38m}K β^+-recoil coincidence experiments

Search for scalar interactions in β^+-ν correlation in ^{38m}K

For details of the apparatus, the fall, 2000 data set, and a table of dominant systematic errors, see last year's Annual Report.

To reach the low systematic errors projected, it has been necessary to include the β^+-ν correlation geometry within a GEANT simulation in order to include small effects due to the β^+'s scattering from the walls. We have shown in the past how we can separate such β^+ recoil coincidences from the true events by kinematic cuts – mostly the time of flight of the recoils – if the β's scatter off materials on the other side of the trap from the β^+ telescope. However, if the β^+ hits the "collimator" near the β^+ telescope before scattering into it (see Fig. 36), this cannot be excluded kinematically. We find we must
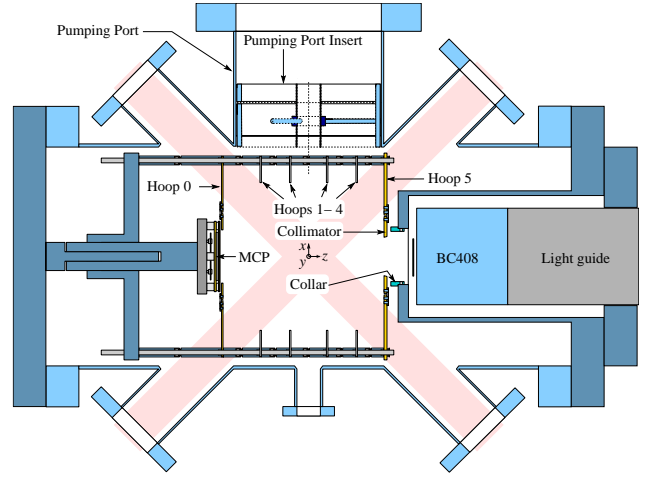

Fig. 36. Top view of present detection trap.

include this scattering to correctly account for the magnitude of the tail of the β^+ response function deduced from the Ar^0 recoil coincidences. This constitutes good indirect evidence of the effect and gives us confidence in the GEANT simulations.

This effect, and other similar scattering effects, produce very small systematic errors in the β^+-ν correlation coefficient a. However, including these effects has been necessary to reach the good confidence levels recently achieved for the fits to the TOF spectra. As was known before, it is impractical to fit the data directly to the full GEANT simulation, because of computation time. Therefore much effort has been expended in producing a Monte Carlo that indirectly includes the GEANT scattering effects without compromising accuracy.

Radiative corrections, mostly from the emission of hard photons produced in the creation of the β^+, are now being indirectly included in the simulations using methods and calculations provided by F. Glück. This should be adequate at the present level of accuracy.

Massive ν admixture search

We have set 90% C.L. limits of $\leq 6 \times 10^{-3}$ on the admixture of ν's having mass 0.7–3.8 MeV with the ν_e produced in β^+ decay. We search for extra TOF peaks in the recoil spectra using maximum likelihood techniques. To achieve this sensitivity, all the position information from the recoil and β^+ detectors, as well as the β^+ energy, is used to reduce the kinematic broadening of the TOF spectra. These are the best direct limits in this mass region for ν's (as opposed to $\overline{\nu}$'s, where $\leq 2 \times 10^{-3}$ was achieved in ^{20}F β^- energy spectrum shape measurements [Deutsch *et al.*, Nucl. Phys. **A518**, 149 (1990)]). There are better indirect limits from the TRIUMF $\pi \rightarrow e\nu_e$ branching ratio [Britton *et al.*, Phys. Rev. Lett. **68**, 3000 (1992)], but this can in principle also be

affected by other new physics. Admixtures with neutrinos in this mass region would affect big bang nucleosynthesis, and can be produced in extra dimension models. M. Trinczek has completed his Ph.D., and we will be submitting a paper for publication shortly.

^{74}Rb charge radius and Q-value

Using the same apparatus and Ti:S laser, we can in principle also trap I=0 ^{74}Rb, which is the isobaric analogue of ^{74}Kr. The ft value of its decay is being studied at TRIUMF and ISOLDE to contribute to CVC and CKM matrix unitarity tests, in a system at higher Z where isospin breaking effects are expected to be larger.

The charge radius is a required input (in the approach used by Towner and Hardy) for the radial wavefunction mismatch correction, the larger of the isospin breaking corrections to the pure Fermi ft values. States with mixed oblate and prolate 0^+ configurations with different dynamic deformation have been shown to occur in even-even nuclei in this mass region, e.g. ^{74}Kr. The difference in dynamic deformation of these configurations is large enough to generate charge radii differences of as large as 0.04 fm or 1.0%, producing a potentially significant uncertainty in the isospin breaking calculations.

The Q-value of ^{74}Rb decay is needed for the ft determination. Once the optimum trap frequency (hence the isotope shift and charge radius) is determined, we hope to determine by our standard β^+-recoil coincidence methods the recoil momentum spectrum, from which the Q-value can be deduced. The fastest Kr recoils have momentum $p_{\max} \approx \sqrt{Q^2 + m_\beta^2} \approx$ Q. For a Fermi decay this is a sharply determined function. ^{74}Rb can be photoionized to determine the trap size and position. By reconstructing the recoil momentum – i.e. not simply taking the recoil TOF – we can narrow the peak and increase the sensitivity. We could reach $\approx$20 keV accuracy in modest beam time, limited by our knowledge of the electric field. The best existing value is 19 keV from ISOLTRAP measurements of the ^{74}Rb mass; 2 keV is eventually needed to achieve 0.1% error in ft.

Spin-polarized measurements for right-handed current search

^{37}K test run

Here we detail the outcome of the November, 2000 ^{37}K polarization tests. Higher polarization has since been achieved and is discussed below.

The polarization scheme presented in the past was partially implemented, in time to make detector tests. The scheme presented has been: 1) turn off trap laser beams and B field; 2) polarize atoms in X direction with optical pumping beam; 3) count; 4) turn on trap to re-confine atoms; 5) repeat.
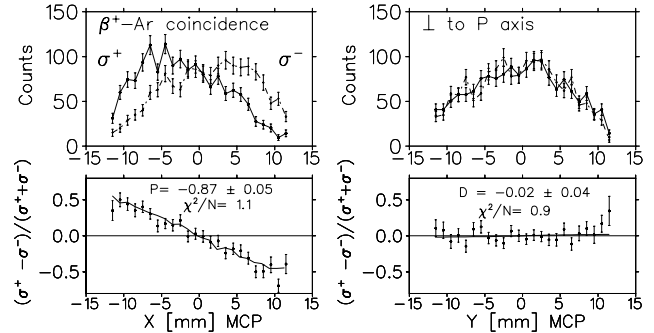

Fig. 37. Asymmetry in MCP position for β^+-Ar coincidences. This asymmetry is dominated by B_ν.

The asymmetries in the X and Y MCP directions are shown in Fig. 37. A clear large asymmetry in the $\hat{x}$ direction is generated; unfortunately, a much smaller but still finite unwanted $\hat{y}$ asymmetry also exists. The symmetry axis was rotated in the analysis to zero the $\hat{y}$ asymmetry. Assuming the standard model, the recoil asymmetry implies that $(87 \pm 5)\%$ nuclear vector polarization was achieved. (The simple atomic probes for ^{41}K in this geometry indicated between 80 and 90% polarization.) A similar polarization is implied by recoil singles data (not shown). If the polarization were known, the recoil asymmetry in coincidence with β's is dominated by the ν asymmetry B_ν in this geometry.

^{41}K 99% polarization

We have since achieved much higher polarization of stable ^{41}K, largely by learning to turn off the trap quadrupole B field, and by improvements in the circular polarization quality of the light. When we optically pump the atoms with a circularly polarized beam tuned to the $4S_{1/2} \to 4P_{1/2}$ "D1" transition, where the ground and excited state angular momenta are the same, the absorption of the beam vanishes when the atoms reach $M_F = F$. Then both the atoms and the nuclei are fully polarized. The vanishing of the fluorescence as a function of time is demonstrated in Fig. 38. Detailed rate equation and optical Bloch equation models then imply that $P \geq 0.99$.

Fluorescence also can vanish via "coherent population trapping", a delicate quantum mechanical effect where the light field couples m_F=0 ground states of some of the atoms into coherent superpositions that
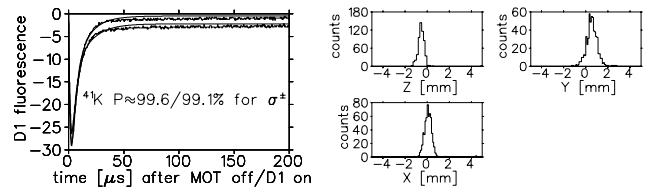

Fig. 38. Left: fluorescence from optical pumping. Right: photoionized ^{38m}K radioactive atom cloud.

do not absorb light, so the atoms are not polarized. The effect is simple to destroy by detuning the laser frequency splitting to more than 100 kHz from the hyperfine ground state splitting. This technique yields remarkably narrow linewidths for an optically driven transition; 10 kHz at our laser powers, with a few Hz achieved elsewhere. We are investigating the possible utility of this technique for ^{36}K and ^{35}K ground state hyperfine splitting measurements. We have characterized the phenomenon and will attempt to publish in an atomic physics journal.

Probing the polarization: non-resonant photoionization

The remaining challenge is to develop direct probes to accurately measure P and the nuclear tensor alignment, both of which are needed for the β^+ decay experiments. The fluorescence curve must be absolutely calibrated using the large signals from ^{41}K atoms, to minimize reliance on atomic physics calculations. Then the fluorescence curve must be measured for ^{37}K, and hopefully ^{36}K, during the measurements. We trap ≈ 1000 ^{37}K atoms, too few for direct fluorescence measurements to be feasible. We have demonstrated a much more sensitive technique, using a nitrogen laser to photoionize the ^{38m}K radioactive atoms (Fig. 38). The ions are then accelerated to the MCP in the electric field. The 337 nm light from the nitrogen laser is sufficient for one-step photoionization from the first excited state of the atoms, not from the ground state. So the photoionization rate is a direct probe of the excited-state population, or the residual non-perfect polarization for the polarized experiments with the $D1$ light on. This presents the unique prospect of monitoring the polarization of the same atoms that are decaying without disturbing their polarization.

We have replaced the present unreliable low-power laser, borrowed from TRIUMF's detector facility, with an economical 355 nm tripled diode-pumped Nd:YAG, a higher-power laser needed to make the fluorescence time curve measurement viable for the small number of ^{37}K and ^{36}K atoms. In addition, we have a 266 nm laser which can photoionize the atoms from their ground state.

^{36}K polarized observables for isospin mixing

We intend to measure in the next scheduling period the isospin mixing between the first two $I^\pi = 2^+$ excited states of ^{36}Ar and the lowest 2^+ $T = 1$ "isobaric analogue" state. We will measure spin-polarized ^{36}K β decay observables. The main purpose is to help test isospin mixing models in the s, d-shell needed for determination of the superallowed Fermi strength (and hence CKM matrix unitarity), as the calculation's methodology is the same.

We will measure the β asymmetry, A_β, and neutrino asymmetry, B_ν. Deviations of these from the value of 1/3 and –1/3 for $2^+ \to 2^+$ pure Gamow-Teller transitions are very sensitive to isospin mixing admixtures [Schuurmans et al., Nucl. Phys. **A672**, 89 (2000)]. The prediction from the isospin mixing methodology performed by Towner is such that A_β is expected to be 0.29 and 0.18 for the two states. The large effect should enable a measurement of the isospin mixing amplitudes to an accuracy of 20% or better. This would be competitive with the best measurements of isospin mixing admixtures to date [Hagberg et al., Phys. Rev. Lett. **73**, 396 (1994)], from branching ratios of 0^+ nuclei to non-analogue transitions, all of which are confined to the f, p-shell.

We have concluded that this is a good first experiment to do with these methods because a measurement with knowledge of the polarization to 3%, and 1% in other systematic errors, will produce a useful result (as opposed to the 0.1% total systematic errors we will need to reach in ^{37}K).

Planned upgrades

The ^{36}K measurement relies on development of polarization methods, β^+ detectors, UHV-compatible optical pumping beam mirrors, and other techniques being developed for the approved ^{37}K parity violation measurements.

Two scintillators will be added to existing ports at 30° to the push beam (Fig. 39). These will be back-to-back with respect to the polarization direction, to minimize systematic errors in the A_β measurement. We plan for each of these to be a phoswich, using plastic scintillator for a fast ΔE and $CaF_2(Eu)$ for the slow (0.96 μs decay time) E detector.
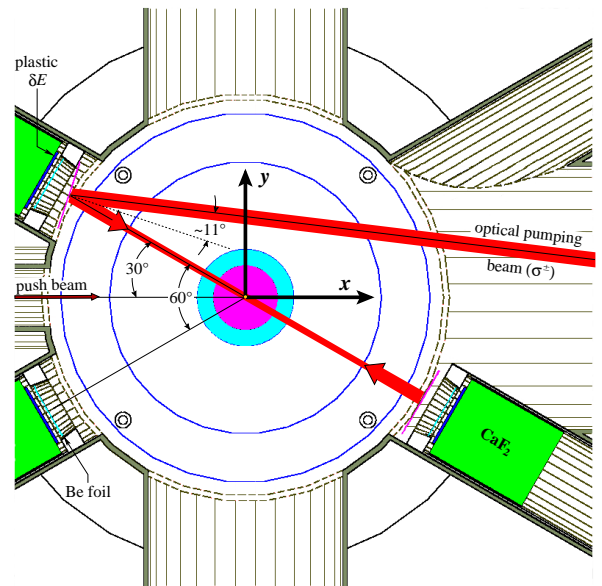

Fig. 39. 2-D side view of planned geometry.

The higher-density CaF_2 (3.16 g/cm^3) allows the 9.8 MeV endpoint β^+ to be contained with a manageable increase in backscatter probability compared to plastic scintillator. We plan to transport the optical pumping light with commercially available multilayer dielectric mirrors mounted on thin substrates (0.1 mm) to minimize β^+ energy loss and angle straggling. A matched pair of mirrors with cancelling angles is necessary to avoid circular polarization distortion from the phase between S and P reflection, and we have demonstrated this technique. We have shown we can switch the trap quadrupole field off quickly enough in the presence of the stainless steel detection chamber.

More laser power is being added to the collection trap, using an existing standing-wave Ti:S and our Ar$^+$ laser retrieved from the parity violating proton scattering experiment. This has increased the trapping efficiency for ^{41}K by a factor of 2, but in a configuration where insufficient frequency stability has been attained. We are converting this to a ring geometry that should enable better frequency locking.

Experiment 744
A kinematically complete study of $\pi^- p \rightarrow e^+ e^- n$
(M.A. Kovash, Kentucky)

Radiative pair production, $\pi^- p \rightarrow e^+ e^- n$, has been shown to be a sensitive probe of the axial structure of the nucleon when studied at low pion energy. Calculations show that at a fixed pion momentum of 160 MeV/c, the shape of the q^2 distribution near its endpoint directly follows the nucleon axial form factor. Accurate measurements of this q^2 distribution can then be used to determine the first moment of the form factor, the axial radius. Experimentally, the value of q^2 can be determined, event by event, by reconstruction from the measured electron and positron momenta. The goal of Expt. 744 is to use the large-acceptance RMC spectrometer to measure the q^2 distribution for radiative pair production at a pion momentum of 160 MeV/c, and, from these data, determine the nucleon axial radius.

During the past year a major milestone in this project has been achieved with the completion of a specially designed liquid hydrogen target. The hydrogen cell and vacuum chamber were developed to minimize the energy loss and straggling of electrons exiting the sides of the cell, while maintaining a large overall target thickness to the beam. Importantly, the target's cantilevered design allows unobstructed detection of electrons over the full range of azimuthal angles. During first beam tests in December, the target, which includes new control, filling and safety systems, was successfully operated without incident.

Due to the small diameter of the target cell, 6 cm, a significant fraction of the pion beam at the focus of the M9A channel falls outside the hydrogen region. Pions which miss the hydrogen affect the cross section normalization, and may produce significant backgrounds if they strike the relatively thick target flanges. In order to track each incident pion into the target region, we have proposed installing MWPCs into the channel at a location directly upstream of the entrance to the RMC spectrometer. Detailed simulations of this geometry are currently under way, but in the interim the wire chambers have been refurbished and chamber mounting hardware has been installed in the channel.

Our previous preliminary radiative pair production data taken with a solid CH_2 target indicate that the observed shape of the q^2 distribution is significantly affected by the energy spread of the pion beam within the target cell. The two most important factors affecting beam energy spread are the irreducible energy acceptance of the channel, and the energy loss of the pion beam in the target assembly. We have proposed to measure the distribution of pion momenta within the hydrogen cell by observing the distribution of momenta of forward-going neutrons from pion charge exchange, $\pi^- p \rightarrow \pi^0 n$. A time-of-flight distribution of cex neutrons directly determines the distribution of incident pion momenta.

To this end, we have made a first attempt at searching for cex neutrons using a new thin scintillation detector with fast timing and neutron-gamma discrimination capabilities. The detector was mounted at a distance of 3 m from the target cell, and TOF spectra were recorded for neutron triggers. The observed distribution shows a large background contribution (the detector was unshielded for this test), but also a distinct feature which is consistent with both the kinematics of charge exchange as well as the expected energy spread of the pion beam. While these first results are encouraging, clearly much work remains to be done to develop this into a reliable diagnostic tool.

Experiment 778
Low energy $\pi^\pm$ differential cross sections in the Coulomb-nuclear interference region with CHAOS
(E.L. Mathie, Regina)

In Expt. 778 the CHAOS collaboration has focused on forward angle $\pi^+ p$ ($\pi^- p$) elastic scattering at low energies. In this angular region there is a dramatic destructive (constructive) interference between the Coulomb scattering and $\pi^+ p$ ($\pi^- p$) hadronic scattering. These data contribute to the broad goals of testing the predictions of chiral-perturbation theory, and determination of the parameters of this fundamental theory. Analyses of πN scattering including this in-

terference region are expected to impact upon the determinations of the πN scattering-amplitudes and the πN Σ-term.

Traditionally measurements in this angular range are complicated by the presence of a halo of muons arising from pions which decay upstream of the detectors. In this experiment a segment of the usual CHAOS CFT array was removed to enable use of a larger, external, array which was positioned to distinguish between pions and muons detected at small angles. The information from this auxiliary array ("The Stack") is interpreted using a neural net. The training or calibrating of the neural net required a whole series of runs at a number of energies around each pion scattering data set energy. In these calibrations, runs with both the whole beam (pions with decay muons) and muon beam (selected by time of flight) were made with the beam passing through each stack counter.

Another distinguishing feature of the experiment was the custom built, planar liquid hydrogen target. In this target a buffer region of hydrogen gas was used to keep the liquid hydrogen thickness uniform across the whole beam width.

The first data for Expt. 778 were obtained in 1999, however, most of the data were obtained in a series of runs throughout 2000. In total some 4.7 TB of data were recorded for seven incident pion energies between 57 MeV (using beam line M11), down to 15 MeV (using M13). Data at 39 MeV were collected using both M13 and M11. In addition, data were collected for the large angle regions of $\pi^+ p$ elastic scattering at 67 MeV.

Since early 2001, the collaboration has been working on the analysis of the data, beginning with analysis of the neural net training data and a very large scale skimming effort. The experimental trigger included rather a large number of muons arising from pion decays in the vicinity of the target, which were removed in the skimming using track information (specifically the momentum versus track angle). In addition, considerable progress was made throughout the year in using the neural net decisions to distinguish between these muons and the pions of interest, scattered to small angles.

It is clear that Monte Carlo simulation of the foreground and background processes is quite important in, for example, determination of the CHAOS and Stack acceptances. The standard GEANT3 based simulation package, CHAOSSIM, was modified in 2001 to incorporate the details of the planar liquid hydrogen target geometry and materials. This plays a particularly important role in the large angle portion of the data, where two structural pillars in the target inhibit scattered pions from reaching the trigger detectors in specific angular regions.
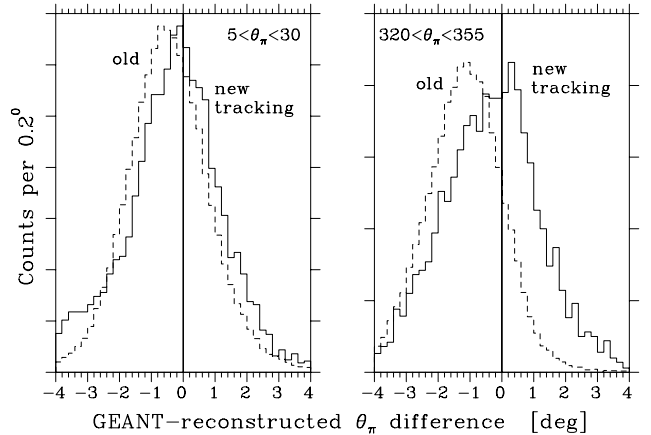

Fig. 40. Histograms of the GEANT-simulated pion scattering angle with the reconstructed value from our analysis using conventional (dashed line) and newly implemented GEANE-based algorithms (solid line) for the most forward scattered particles.

In the forward angle region accurate scattering angle determination is very important because the cross sections vary extremely rapidly. In order to optimize the CHAOS scattering angle resolution, a new track fitting scheme based upon GEANE has been implemented. In this scheme the GEANT representation of all of the detectors (already developed for the Monte Carlo) is used to determine particle energy loss along the track. Generally this algorithm provides a better momentum, scattering angle and vertex determination, shown in Fig. 40.

Analysis of Expt. 778 continues in 2002.

Experiment 801
Studies of multi-phonon states via β-decay
(R.F. Casten, Yale)

The aim of Expt. 801 is to investigate the collective phonon and multi-phonon structure of low-lying intrinsic excitations in rotational nuclei. β-decay from a low-spin parent is an effective method for the population of low-spin members of these bands. Accurate measurement of low-intensity γ-ray transitions is of central importance in the interpretation of these excitations. The use of a compact configuration of large-volume Ge detectors, for efficient γ-γ coincidence spectroscopy, coupled with the high intensity and high isotopic purity beams available at ISAC, provides a much higher sensitivity than was available in the previous generation of experiments.

An experiment to study ^{162}Er was carried out in 2000 at the ISAC GPS β-decay end station. The ^{162}Er nuclei were populated through the β-decay of ^{162}Yb and studied through γ-ray spectroscopy. (The details of this experiment are described in the 2000 Annual Report.)

This nucleus is of special interest since the 2^+ member of the $K^\pi = 0_2^+$ band (at 1171 keV) is reported to decay with collective strength to the ground state band, and so this excitation would seem a likely candidate for being a β-vibration: The $B(E2; 2_{K=0}^+ \to 0_g^+)$ strength [Ronningen $et\ al.$, Phys. Rev. **C26**, 97 (1982)] corresponds to a squared intrinsic matrix element $|\langle K^\pi = 0_2^+|E2|K^\pi = 0_g^+\rangle|^2 = 8.0(15)$ W.u., which is comparable to the largest such values in the rare earth region and fully half as large as for the γ-vibrational excitation in this nucleus. The literature values [de Boer $et\ al.$, Nucl. Phys. **A236**, 349 (1974)] for the relative $B(E2)$ strengths of the transitions depopulating this level $(2_{K=0}^+ \to 0_g^+, 2_g^+, 4_g^+)$, however, deviate from the Alaga rules by nearly an order of magnitude. These anomalous results have precluded any simple interpretation of the intrinsic structure of the $K^\pi = 0_2^+$ excitation in ^{162}Er and have called the validity of a pure rotational interpretation of this excitation into doubt.

The present measurements of the decay properties of the $K^\pi = 0_2^+$ excitation (Fig. 41) substantially revise the γ-ray branching data. The relative intensities of the transitions depopulating the $2_{K=0}^+$ level can be obtained in a straightforward fashion from spectra gated upon transitions feeding the $2_{K=0}^+$ level (Fig. 42). With the newly measured intensities, the $B(E2)$ values for
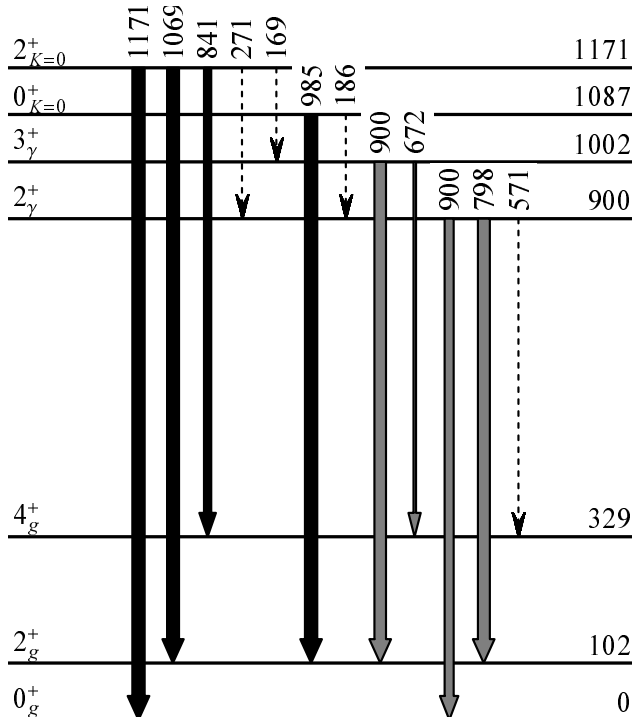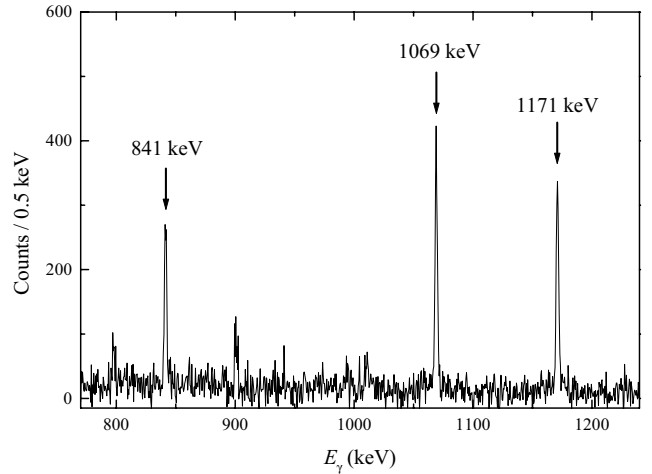

Fig. 42. Composite spectrum gated upon transitions feeding the $2_{K=0}^+$ level at 1171 keV, showing the 841, 1069, and 1171 keV branches from this level.

the branches from the $2_{K=0}^+$ level are found to be in reasonably good agreement with the Alaga rules. The measured $B(E2; 2_{K=0}^+ \to 4_g^+)/B(E2; 2_{K=0}^+ \to 0_g^+)$ ratio is 3.1(2). The deviation of this from the Alaga value of 2.6 can be attributed to relatively minor mixing effects; in contrast, the literature ratio of 20(15) would have pointed towards extreme mixing of the $K^\pi = 0^+$ band with other bands or a breakdown of the rotational picture. The present results suggest the $K = 0_2^+$ excitation in ^{162}Er is now a viable candidate for a β-vibrational excitation.

The only other low-lying $K^\pi = 0^+$ excitation in ^{162}Er identified in the literature is based upon a spin assignment of (0^+) for a level at 1420 keV. This excitation, from its reported decay properties, would have been of interest as a possible two-γ-phonon excitation candidate. The present coincidence data, however, show the existence of a weak 418 keV transition from the level at 1420 keV to the 3^+ member of the γ band. The existence of such a transition is inconsistent with a 0^+ assignment for the level. A tentative spin assignment of 2^-, based upon the level's decay properties, is reasonable in the context of the octupole excitation systematics for the region.

Experiment 823
Pure Fermi decay in medium mass nuclei
(G.C. Ball, TRIUMF)

Precise measurements of the intensities for superallowed Fermi $0^+ \to 0^+$ β decays have provided a demanding test of the CVC hypothesis at the level of 3×10^{-4} and also led to a result in disagreement with unitarity (at the 98% confidence level) for the CKM

Fig. 41. Decay scheme for the low-spin members of the ground, γ, and $K^\pi = 0_2^+$ bands in ^{162}Er obtained from the present work. Arrow widths are proportional to γ-ray intensity, normalized to the strongest transition from each level. Unobserved transitions for which intensity limits were obtained are indicated by dashed arrows.

matrix [Towner and Hardy, WEIN'98 (World Scientific, Singapore, 1999) p. 318]. Since this would have profound implications for the minimal standard model, it is essential to address possible "trivial" explanations for this apparent non-unitarity, such as uncertainties in the theoretical isospin symmetry-breaking correction. Uncertainties in the calculated Coulomb corrections can be studied by extending the precision β decay measurements to heavier ($A \geq 62$, $T_z = 0$) odd-odd nuclei where these corrections are predicted to be much larger [Ormand and Brown, Phys Rev. **C52**, 2455 (1995)]. The primary goal of the Expt. 823 experimental program is to measure the half-lives and branching ratios for the superallowed β decay of these radioactive nuclei produced at ISAC. The early measurements have focused on ^{74}Rb (see 1999 and 2000 Annual Reports).

High precision β decay branching ratio measurements for ^{74}Rb

Since the Q_{EC} values are large for the heavier $T_Z = 0$ nuclei, there are a large number of excited $(0,1)^+$ states in the daughter nucleus that could be populated by β decay. This so-called "pandemonium effect" [Hardy *et al.*, Phys. Lett. **B17**, 107 (1977)] could confound an accurate determination of the superallowed transitions if these highly excited states in the daughter nucleus decay directly to the ground state. These measurements are also demanding because of the short half-lives (<100 ms) and limited beam intensities. Two experiments were carried out at ISAC in 2000–2001 to search for allowed non-analogue transitions in the β decay of ^{74}Rb to excited $(0,1)^+$ states in ^{74}Kr. The first experiment was carried out using a technique similar to that described previously [Hagberg *et al.*, Nucl. Phys. **A571**, 555 (1994)]. In this case, a fast tape transport system was used to collect and move the ^{74}Rb samples out of the vacuum chamber and position them between two plastic scintillator paddles each backed by a large ($\sim$80%) HPGe detector mounted collinearly (see the 2000 Annual Report for a more complete description of this experiment). One difficulty in this measurement was the background coming from the decay of ^{74}Ga, a long-lived ($t_{1/2} = 8.12$ ms) contaminant beam which determined the limit for detecting very weak high-energy γ-rays from the β decay of ^{74}Rb. However, weak Gamow-Teller/Fermi decays to one or more high-lying levels in ^{74}Kr were observed by their depopulation through the known first excited 2^+ level at 456 keV. This result indicates that the superallowed branch is the dominant transition (>99%), similar to those observed previously for odd-odd $T_Z = 0$ superallowed decays.

The determination of the transition strengths for non-analogue $0^+ \rightarrow 0^+$ decays provides a critical test of the model predictions for the isospin mixing component of the Coulomb correction for superallowed β decays. Recently, in-beam experiments [Chandler *et al.*, **C56**, R2924 (1997); Becker *et al.*, Eur. Phys. J. **A4**, 103 (1999)] have revealed the existence of a low-lying, isomeric 0_2^+ level in ^{74}Kr at 508 keV which decays primarily by an electric monopole transition to the ground state of ^{74}Kr. A preliminary experiment to search for the β decay of ^{74}Rb to this excited 0_2^+ level was carried out in May–June, 2000 at a new target station, GP2, provided by TRIUMF. In this measurement the ^{74}Rb atoms were implanted into a 6 mm wide mylar tape of a moving tape transport system that operated in vacuum. The collection point was viewed by two large plastic scintillation counters (one thin ΔE counter and one thick E counter) to detect positrons, three LN-cooled Si(Li) diodes for the detection of conversion electrons and an ($\sim$80%) HPGe detector for γ-rays. Both Si(Li)-plastic and Ge-plastic coincidence data were recorded (see the 2000 Annual Report for a more complete description of this preliminary experiment). Before the production run in May, a number of improvements in the experimental hardware were made including: 1) the installation of a wider (13 mm) tape transport system to ensure that all of the implanted activity is deposited on the tape; 2) the fabrication of a hollow light guide for the thin ΔE scintillator which resulted in a factor of three reduction in 511 keV γ-rays in the β-coincident HPGe spectrum; and 3) the three Si(Li) detectors were replaced by two Si(Li) detectors mounted symmetrically above and below the tape collection spot to improve the conversion electron detection efficiency. Plans to operate the mass separator in the high-resolution mode to significantly reduce the isobaric contaminant ^{74}Ga could not be carried out because of difficulties with the ISAC target ion source. Nevertheless, the quality of the production run data was improved substantially over that obtained in the preliminary run. Data analysis is still in progress.

Weak transitions were observed in the Si(Li) spectra at 39 and 495 keV corresponding to the decay of the 508 keV level to the ground state and first excited 2^+ level in ^{74}Kr (see Fig. 43). In addition, ^{74}Rb β-delayed γ-rays were observed at 456, 1198, 1233 and 4244 keV (see Fig. 44). These results are in disagreement with a recent ISOLDE measurement [Oinonen *et al.*, Phys. Lett. **511B**, 145 (2001)] which observed the 495 keV electron transition at about the same intensity but did not observe any γ-rays. Our data have been incorporated into the partial decay scheme shown in Fig. 45. The upper limit for the non-analogue β decay branch ($< 3 \times 10^{-4}$) is far smaller than previously predicted [Ormand and Brown, *op. cit.*] Recently, shell model calculations have been carried out that included the promotion of two particles to the g-d shell [Towner and
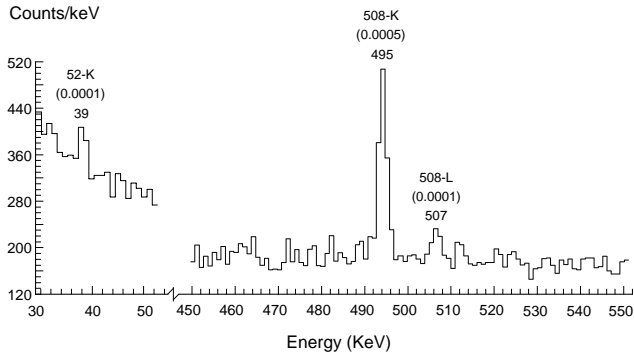
Fig. 43. Parts of the β-coincident conversion electron spectrum measured with the Si(Li) diodes. The numbers in parentheses represent the approximate intensities of the transitions per ^{74}Rb decay.

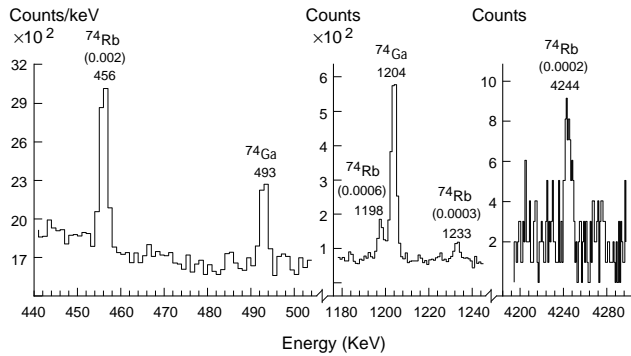Fig. 44. Parts of the β-coincident γ-ray spectrum measured with HPGe detector. Numbers in parentheses represent the approximate intensities of the transitions per ^{74}Rb decay.

Fig. 45. The ^{74}Rb decay scheme. The numbers in parentheses are approximate intensities of the transitions per ^{74}Rb decay.

Hardy, private communication and to be published]. In this model space, with an adjustment of the effective interaction, it was possible to get the first excited 0^+ state at $\sim$0.5 MeV in ^{74}Kr with a small branching ratio consistent with the present data. These same calculations also predict that a large number of excited 1^+ states are populated at 4–6 MeV excitation in ^{74}Kr with five levels carrying three-quarters of the total decay strength of $\sim$0.9%. The calculations also indicate that about half of the decay strength from these 1^+ levels feeds the first excited 2^+ level, while 24% and 16% directly feed the ground and first excited 0^+ states, respectively. While these predictions are qualitatively in agreement with experiment, further theoretical and experimental studies are needed. In particular, detailed spectroscopy measurements using the reconfigured 8π spectrometer are planned [Svensson *et al.*, TRIUMF Expt. 909].

Outlook

During the coming year the objectives are: 1) to complete the analysis of the precision branching ratio measurement for the decay of ^{74}Rb and submit a paper for publication and 2) to measure the transition strength of the non-analogue $0^+ \rightarrow 0^+$ branch in ^{38m}K.

Experiment 824
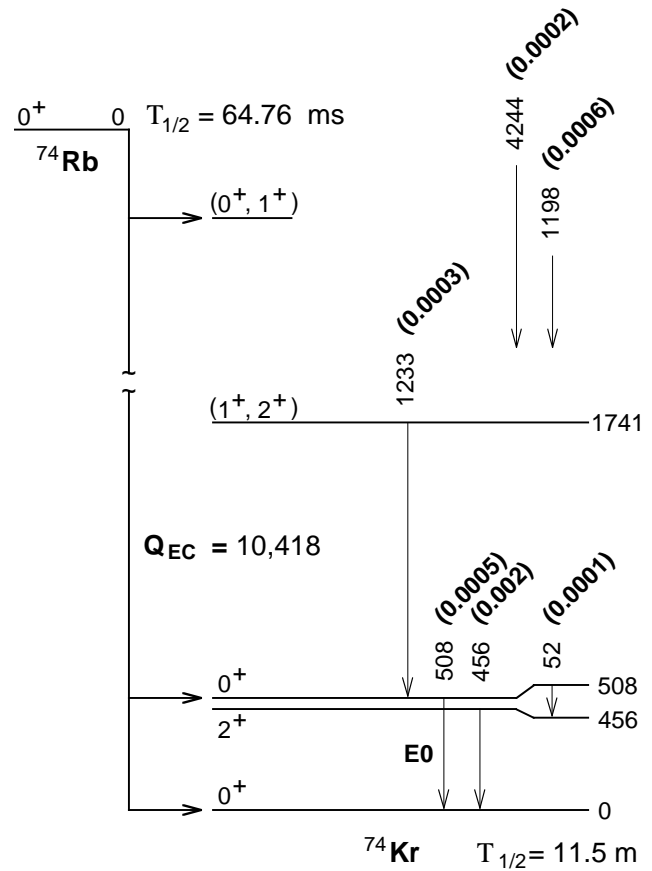
Measurement of the astrophysical rate of the ^{21}Na(p, γ)^{22}Mg reaction
(J.M. D'Auria, SFU)

Experiment 824 has initiated the data-taking phase using the new DRAGON facility in 2001. The objective of this experiment is to measure, with a precision of 20% or better, the astrophysical rate of the reaction ^{21}Na(p, γ)^{22}Mg at explosive stellar temperatures. This reaction is thought to play a key role in the production and destruction of the long-lived isotope ^{22}Na during nova and X-ray bursts. Unsuccessful searches in the universe for the observation of its unique decay γ-ray using γ-ray observatories in such cataclysmic events have indicated that present nova models require improvement. In the energy region of interest such radiative proton capture reactions are governed primarily by narrow resonances, requiring direct and indirect studies to elucidate.

This experiment is performed on the new DRAGON facility (see the Experimental Facilities section of this Annual Report) just installed on the HEBT-2 beam line at ISAC. The system consists of

a windowless gas target in which Expt. 824 uses hydrogen gas, surrounded by a BGO gamma detector array, a recoil mass separator to separate the rare reaction products from the relatively more intense beam particles, and a focal plane detection system to detect the separated reaction products. The focal plane detection system can be either a simple charged particle detector such as a silicon strip detector, or a more sophisticated package consisting of a micro channel plate/electron system to produce a start signal and a large volume ionization chamber with front end, parallel plate avalanche counter to provide an energy and a stop signal.

In the gas target a distribution of charge states is created of both the beam and the reaction products. The charge state of interest is then selected in the first dipole of DRAGON (MD1). In earlier studies the charge distribution of low energy heavy ions resulting from passage through a gas system was studied [W. Liu, M.Sc. thesis (Simon Fraser University, 2001)]. Table VIII presents a summary of some of these data obtained using the DRAGON windowless gas target and also taken using a similar system at the University of Naples.

The reaction products are then separated from the beam particles using the first electrostatic dipole unit, ED1, taking advantage of the small energy difference ($\approx$4.5%). In the second stage of DRAGON, a second separation stage using further magnetic and electrostatic elements is then performed. Around the gas target, an array of 29 BGO gamma detectors is positioned to observe the prompt reaction gammas (E$\geq$2 MeV in this study) both singly and in coincidence; this can provide an additional factor to further suppress beam background in the recoil detector.

Further discussion on the operation of DRAGON and details of the system can be found on pg. 131 of this Annual Report.

Over the course of the last 12 months the following studies were undertaken as part of the preparation for data-taking. The commissioning of DRAGON was initiated using the ^{15}N$(p, \alpha\gamma)^{12}$C and ^{21}Ne$(p, \gamma)^{22}$Na reactions. The former was used to determine the pressure/density profile in the windowless gas target (see pg. 132, Fig. 124 of this Annual Report) and the latter reaction was used both to test the operation of the entire system as well as to provide an initial estimate of its transmission.

In the ^{21}Ne$(p, \gamma)^{22}$Na reaction, resonances with $E_{\mathrm{cm}} = 258.3/259.3$ and 732.7 keV were studied. The measured resonance strengths ($\omega\gamma$) were within one standard deviation of literature values. In these studies a double sided, silicon strip (16 + 16 strips) detector (DSSSD) was used to detect the separated recoils

and the gamma array was used to provide a coincident signal with the prompt reaction gammas.

A radioactive beam with intensities up to 5×10^8/s was made available from the ISAC system to initiate measurements of the ^{21}Na$(p, \gamma)^{22}$Mg reaction in inverse kinematics. Using a hydrogen target thickness of about 4×10^{18} atoms/cm^2, prompt reaction gammas were detected with the BGO gamma array, and separated reaction products detected with the DSSSD. Figure 46 displays a composite spectrum collected for two different runs. Initially, a high charge state (11+) of the ^{21}Na beam was transmitted through DRAGON and used to calibrate the DSSSD. Following this, the ^{22}Mg recoils (5+ charge state) from the ^{21}Ne$(p, \gamma)^{22}$Na reaction were transmitted to the DSSSD. The lower peaks in the spectrum arise from an alpha calibration source.

Over a series of runs a special diagnostic to minimize the amount of beam spill into the gamma array around the target was developed and efforts taken to optimize the beam transmission and minimize the background radiation into the array.

Yield measurements (recording singles and coincident gamma signals simultaneously) were performed by scanning the beam energy around the known state reported previously in ^{22}Mg at $E_{\mathrm{cm}} = 212$ keV, and, in addition, scanning in energy a strong resonance observed at $E_{\mathrm{cm}} \approx 822$ keV. These data are still under analysis. Further study of the operational performance of the entire DRAGON facility is presently in progress.
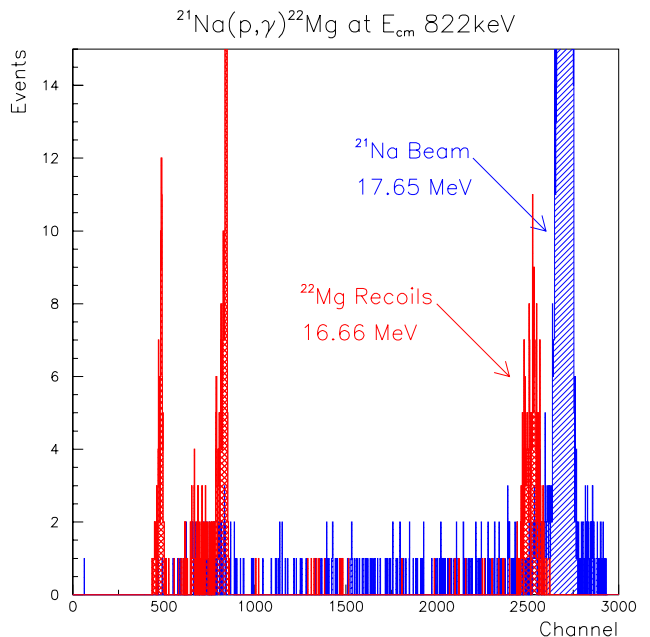

Fig. 46. Composite figure from two separate runs of reaction recoils and the ^{21}Na beam (11+). See text.

Table VIII. Experimental equilibrium charge state fractions (%), where $*$ and † refer to data from University of Naples and DRAGON measurements, respectively.

	E(MeV/u)	q_{in}	n(1+)	n(2+)	n(3+)	n(4+)	n(5+)
^{15}N+H$_2$†	0.435	4+				3.70 ±0.22	34.32±0.90
^{16}O+H$_2$*	0.138	2+,3+,4+	10.46±0.56	43.30±1.21	38.99±1.18	7.01±0.46	0.33 ±0.05
^{16}O+H$_2$*	0.200	3+,4+,5+		17.59±0.71	48.78±1.21	30.17±1.05	3.41±0.27
^{16}O+H$_2$*	0.325	3+,5+		1.10±0.09	13.41±0.56	47.59±1.22	34.19±1.13
^{16}O+H$_2$†	0.325	4+			7.37±0.41	50.07±0.94	37.51±0.91
^{16}O+H$_2$*	0.500	4+			0.50±0.06	10.00±0.44	44.50±1.27
^{16}O+H$_2$†	0.500	4+			0.35±0.04	9.89±0.54	41.88±0.95
^{16}O+H$_2$*	0.588	3+			0.11±0.02	3.50±0.29	32.23±1.17
^{16}O+H$_2$†	0.800	4+				0.36±0.04	8.93±0.51
^{23}Na+H$_2$*	0.200	3+,5+,6+		7.39±0.49	42.51±1.21	40.78±1.20	8.72±0.57
^{23}Na+H$_2$*	0.374	4+,6+			1.01±0.11	13.25±0.54	40.90±1.15
^{23}Na+H$_2$*	0.478	4+,7+			0.10±0.02	2.18±0.15	16.74±0.66
^{24}Mg+H$_2$†	0.200	6+			36.17±0.88	48.72±0.94	14.03±0.44
^{24}Mg+H$_2$†	0.500	6+				0.66±0.08	8.29±0.40
^{24}Mg+H$_2$†	0.800	6+					
^{16}O+He*	0.138	2+,3+,4+	20.78±0.79	44.96±1.18	27.69±0.97	6.31±0.35	0.26±0.04
^{16}O+He*	0.200	3+,4+,5+	0.02±0.003	33.04±1.10	46.31±1.22	18.64±0.74	1.92±0.15
^{16}O+He*	0.325	3+,5+		7.90±0.43	34.48±1.10	42.28±1.17	14.61±0.59
^{16}O+He*	0.371	3+		4.82±0.27	25.56±0.93	47.21±1.47	20.31±0.78
^{16}O+He*	0.588	3+			3.90±0.22	24.45±0.90	47.52±1.19
^{16}O+He*	0.750	6+				9.00±0.59	37.38±1.19
^{16}O+He*	0.875	5+					29.88±1.11

Table VIII. Continued.

	E(MeV/u)	q_{in}	n(6+)	n(7+)	n(8+)	n(9+)	n(10+)
^{15}N+H$_2$†	0.435	4+	57.57±0.95	4.41±0.26			
^{16}O+H$_2$*	0.138	2+,3+,4+					
^{16}O+H$_2$*	0.200	3+,4+,5+	0.05±0.01				
^{16}O+H$_2$*	0.325	3+,5+	3.71±0.29				
^{16}O+H$_2$†	0.325	4+	5.05±0.35				
^{16}O+H$_2$*	0.500	4+	43.50±1.26	1.50±0.09			
^{16}O+H$_2$†	0.500	4+	46.77±0.96	1.11±0.07			
^{16}O+H$_2$*	0.588	3+	59.85±1.24	4.31±0.30			
^{16}O+H$_2$†	0.800	4+	65.81±0.84	23.78±0.72	1.12±0.14		
^{23}Na+H$_2$*	0.200	3+,5+,6+	0.60±0.07				
^{23}Na+H$_2$*	0.374	4+,6+	34.69±1.09	9.44±0.50	0.71±0.08		
^{23}Na+H$_2$*	0.478	4+,7+	40.18±1.14	32.81±1.06	7.50±0.48	0.49±0.08	
^{24}Mg+H$_2$†	0.200	6+	1.07±0.06	0.01±0.001			
^{24}Mg+H$_2$†	0.500	6+	30.45±0.76	40.81±0.85	17.66±0.51	2.13±0.12	
^{24}Mg+H$_2$†	0.800	6+	1.40±0.08	10.51±0.33	41.64±0.89	37.78±0.86	8.67±0.42
^{16}O+He*	0.138	2+,3+,4+					
^{16}O+He*	0.200	3+,4+,5+	0.07±0.01				
^{16}O+He*	0.325	3+,5+	0.73±0.08				
^{16}O+He*	0.371	3+	2.10±0.12				
^{16}O+He*	0.588	3+	23.31±0.87	0.82±0.09			
^{16}O+He*	0.750	6+	48.11±1.25	5.51±0.31			
^{16}O+He*	0.875	5+	59.44±1.22	10.68±0.59			

Experiment 838
Double radiative capture on pionic hydrogen
(RMC Collaboration)

Negative pions stopped in hydrogen form pionic hydrogen atoms. These atoms can disintegrate via several modes that include the well known processes of charge exchange $\pi^- p \to \pi^0 n$, radiative capture $\pi^- p \to \gamma n$, and pair production $\pi^- p \to e^+ e^- n$.

However, for pionic hydrogen an additional mode of capture is predicted by theory

$$\pi^- p \to \gamma\gamma n \,.$$

The predicted branching ratio is 5.1×10^{-5}, with a mechanism that is dominated by the annihilation of the stopped, real π^- on a soft, virtual π^+, i.e. $\pi\pi \to \gamma\gamma$. It thereby offers a novel window on the $\pi\pi \to \gamma\gamma$ vertex and the proton's pion field.

In Expt. 838, using the RMC spectrometer on the M9A beam line, we have conducted the first measurement of double radiative capture on pionic hydrogen. Incoming pions were counted in a plastic scintillator telescope and stopped in a liquid hydrogen target. Outgoing photons were detected by pair production in a cylindrical Pb converter and electron-positron tracking in cylindrical multiwire and drift chambers. We employed a two-photon trigger based on the hit multiplicities and the hit topologies in the trigger scintillator rings and the drift chamber cells.

The major backgrounds were real γ–γ coincidences arising from $\pi^0 \to \gamma\gamma$ decay and accidental γ–γ coincidences arising from simultaneous π^- stops. To reject the π^0 background we imposed a photon opening angle cut of $\cos\theta > -0.1$, and to reject the multi-π background we imposed a beam telescope amplitude cut. This yielded a total of 544 events from double radiative capture on pionic hydrogen.

After accounting for the number of stopped pions and the acceptance of the RMC detector we obtained a branching ratio for double radiative capture on pionic hydrogen of $(3.08 \pm 0.13(\text{stat.}) \pm 0.31(\text{syst.})) \times 10^{-5}$. A comparison of the corresponding photon opening angle distributions from experiment and theory is shown in Fig. 47. Our measured branching ratio and opening angle distributions are in reasonable agreement with the theoretical predictions. In particular our result supports the theoretical prediction of a dominant $\pi\pi$ annihilation mechanism.
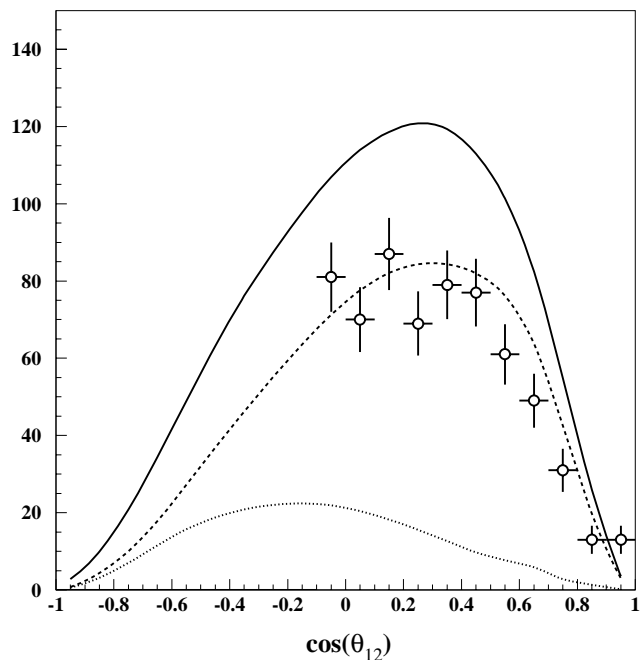

Fig. 47. Comparison of the opening angle distribution from the experimental data and the theoretical calculation. For theory the dashed curve is the $\pi\pi$ annihilation process, the dotted curve is the NN bremsstrahlung process, and the solid curve is the full calculation. These curves are convoluted with the response function of the RMC spectrometer.

Experiment 862
Analyzing powers in the $\vec{p}(\pi, \pi\pi)$ reactions with CHAOS
(E.L. Mathie, Regina)

Chiral perturbation theory (ChPT) is considered the most important effective field theory applied at low energies. Some argue that ChPT *is* QCD at low energies. Experimental descriptions of interactions involving pions and nucleons provide important tests of ChPT. To date, applications of ChPT for the pion induced pion production reactions have only been tested by total and differential cross sections. In his M.Sc. thesis, K. Babcock has argued that total cross sections do not provide adequate constraints to uniquely determine the parameters of the theory, the low energy constants (LEC). In Fig. 48 a number of statistically equivalent fits to total cross sections are shown. In addition it remains possible that third order theory may be insufficient to describe the details of the differential cross section distribution, which were not successfully fit. Polarization dependent quantities offer independent constraints from total and differential cross sections, and it is hoped determination of such quantities may help to address the question of convergence of the theory at third order, and hopefully to determine values for the low energy constants (LEC) of the theory, which must come from experiment.
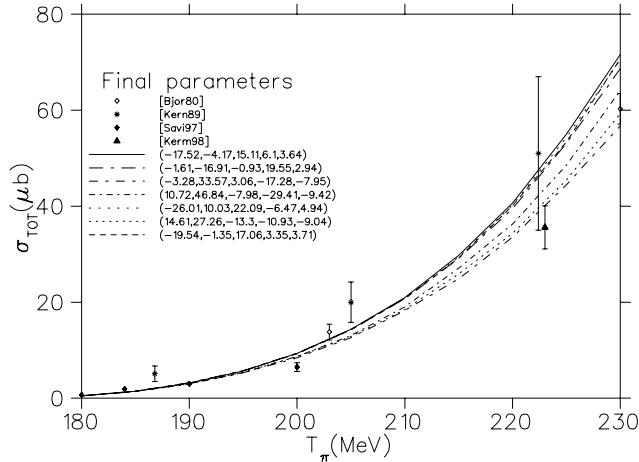
52

Fig. 48. The total cross sections for $p(\pi^-, \pi^+\pi^-)n$ vs. incident kinetic energy with a variety of equivalent fitted distributions [Babcock, 2001]. The values of the LECs for each fit are shown in the legend.

In Expt. 862, the first measurements of the asymmetry A in the $\vec{p}(\pi, \pi\pi)$ reactions will be obtained. The CHAOS spectrometer will be used to observe the incident and outgoing charged particles after interaction in the CHAOS polarized proton target (CPPT), which was previously used in Expt. 560. This asymmetry is defined in terms of the differential cross sections σ^+ (σ^-) for positive (negative) target polarization according to

$$A = \frac{1}{P_{\text{tgt}}} \frac{\sigma^+ - \sigma^-}{\sigma^+ + \sigma^-}$$

where P_{tgt} refers to the magnitude of target polarization and σ refers to any one of several differential cross sections which may be determined. In earlier CHAOS experiments, such as Expt. 624, it has been demonstrated that the differential distributions for $(\pi, \pi\pi)$ reactions can be expressed in terms of: the square of the dipion invariant mass, $M_{\pi\pi}^2$; the square of the momentum transfer to the nucleon, t; and the angle between the two final state pions in the dipion system. The fourth kinematical variable, x (the angle between the dipion and the plane defined by the incident pion and outgoing nucleon), is not well covered in the CHAOS acceptance and hence must be modelled.

The most recently completed CHAOS experiment, Expt. 778, required a unique small scattering angle configuration in which part of the spectrometer was not utilized. In addition, during the two years of operating Expt. 778, significant improvements were made to the data acquisition system, including the replacement of a programable hardware second level trigger with software (VME) equivalent trigger. It was thus necessary for the CHAOS collaboration to begin Expt. 862 with a lengthy recommissioning of the spectrometer during May and June, 2001 in order to recommission the full horizontal angle acceptance of the spectrometer and adapt the software triggers to the pion production experiment. At the same time all of the detectors were retuned and a major reorganization of the spectrometer electronics was accomplished.

The procedure to use the CPPT in CHAOS involves polarizing the target in an external, high homogeneity solenoid; transporting the target with an internal polarization holding field into the spectrometer; and then using the spectrometer field to maintain the frozen target polarization throughout the reaction studies. The decay of the target polarization is a strong function of the CHAOS field. In our pion elastic scattering experiments, the CHAOS field was higher than what was used in the earlier $p(\pi, \pi\pi)$ studies, so the recommissioning run included considerable running with CH_2 targets to investigate the effect of operating at a higher field on the acceptance. These results are being analyzed, and will help determine the detailed goals for running in 2002.

The improvements in triggering and data acquisition rate meant that triggers caused by a pion and proton in the final state, which were rejected in our earlier $(\pi, \pi\pi)$ experiments by a high momentum cut, could now be accepted. In an effort to make use of this additional capability, an investigation of the feasibility of triggering on for example, $p(\pi^-, \pi^- p)\pi^0$, was undertaken. Although the reaction could be identified, it is unlikely that sufficient statistics above background could be obtained within the running constraints of Expt. 862 to realize the additional goal of determining an analyzing power for this channel.

Unfortunately, TRIUMF was unable to recommission the CPPT in time for running in 2001, so data runs were necessarily postponed until 2002. Work was, however, begun on the target with new control software and upgrades to the pumping systems. Operation of Expt. 862 continues in 2002.

Experiment 863
Ground state magnetic moments of ^{75,77,79}Ga (LTNO)
(P. Mantica, MSU)

The focus of Expt. 863 is to study the evolution of the single-particle structure of medium-mass nuclides above $_{28}$Ni toward the $N = 50$ shell closure. A well-known shape transition from spherical to moderate deformation ($\beta_2 \approx 0.2$) occurs in the neutron-rich $_{31}$Ga and $_{32}$Ge isotopes between $N = 40 - 42$. Since the ground state magnetic dipole moment can serve as a sensitive probe of the nuclear ground state wavefunction, the experimental determination of the magnetic moments of heavy, odd-A Ga isotopes can address the extent to which quadrupole deformation persists toward $N = 50$.

53

A low-energy beam of ^{75}Ga was produced at the TRIUMF-ISAC facility using a surface ion source equipped with a Ta production target. An average proton beam current of 20 μA was maintained on the Ta target. The ^{75}Ga nuclei were implanted into an iron foil mounted on a cold finger inside the ^{3}He/^{4}He dilution refrigerator. No evidence of other $A = 75$ isobar contaminants was observed in the low-energy radioactive beam.

The nuclear orientation of ^{75}Ga was monitored by measuring the angular distribution of β particles emitted from the radioactive parent (T$_{1/2}(^{75}$Ga) = 126 s). Two plastic scintillator ΔE-E telescopes were placed at 0° and 180° relative to the external magnetic field provided by a superconducting split-coil magnet surrounding the ^{75}Ga implantation position. The detectors were mounted external to the dilution refrigerator cryostat, 10.3 cm from the centrepoint of the implantation foil. The energies of the ^{75}Ga β particles, Q_β(max) = 3.4 MeV, are sufficient to ensure that a large fraction of these particles pass through the thin cryostat walls. Three Ge detectors were also placed around the sample position at 0°, 90°, and 180° relative to the external magnetic field. These detectors were used to monitor the γ-rays emitted from the ^{60}Co<u>Fe</u> thermometer placed on the cold finger to monitor the temperature of the sample. The Ge detectors were also used to monitor the ^{75}Ga γ-ray activity.

Warm ($T > 1$ K) and cold ($T < 15$ mK) data were collected at an external magnetic field of 0.2 T to determine the fractional polarization of the implanted ^{75}Ga sample. The observed β particle asymmetry was 15%. To confirm polarization of the ^{75}Ga sample, the external field was reversed, and a corresponding reversal of the β particle asymmetry was observed. These data are shown in Fig. 49.

Radio frequency scans over the range 85 to 175 MHz were completed. This range covers g-factor values between 1.0 and 2.1 for ^{75}Ga, taking the known hyperfine field of Ga in iron to be –11.0(3) T. These data are currently under analysis.

Experiment 864
Dibaryon search by double radiative capture on pionic deuterium
(RMC Collaboration)

At present the deuteron is the only established particle with a baryon number $B = 2$. However, a large number of theoretical predictions for additional dibaryons have been published in the literature. Obviously the experimental discovery of another dibaryon would provide new insight into meson-baryon and quark-gluon dynamics at the GeV scale.

A recent claim for dibaryon production in proton-proton double bremsstrahlung reaction $pp \rightarrow pp\gamma\gamma$ has been published by the Di2γ collaboration at the JINR phasetron. Specifically, they reported an intriguing double-peaked structure in the energy spectrum of the coincident γ-ray events from the $pp \rightarrow pp\gamma\gamma$ reaction. They attributed the structure to the d^* dibaryon of mass 1959 ± 6 MeV and width ≤ 8 MeV, which was first produced via the two-body process $pp \rightarrow d^*\gamma$ and then decayed via the three-body process $d^* \rightarrow pp\gamma$.

Recently Gerasimov suggested that double radiative capture on pionic deuterium

$$\pi^- d \rightarrow nn\gamma\gamma$$
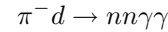
is an excellent candidate for the further investigation of the dibaryon's existence. In the equation, the d^* dibaryon is first produced via radiative capture $\pi^- d \rightarrow d^*\gamma$ and then disintegrates via radiative decay $d^* \rightarrow nn\gamma$. Using a simple model, Gerasimov estimated that the branching ratio for the d^*-mediated process may be as large as a few tenths of one per cent. This yield would exceed by 100 times the expected two-photon branching ratio for non-resonant double radiative capture.

In Expt. 864, using the RMC spectrometer on the M9A beam line, we have performed a dedicated search for dibaryon production via double radiative capture on pionic deuterium. Incoming pions were counted in a plastic scintillator beam telescope and stopped in a liquid deuterium target. The outgoing photons were detected by pair production in a cylindrical lead converter and electron-positron tracking in a cylindrical
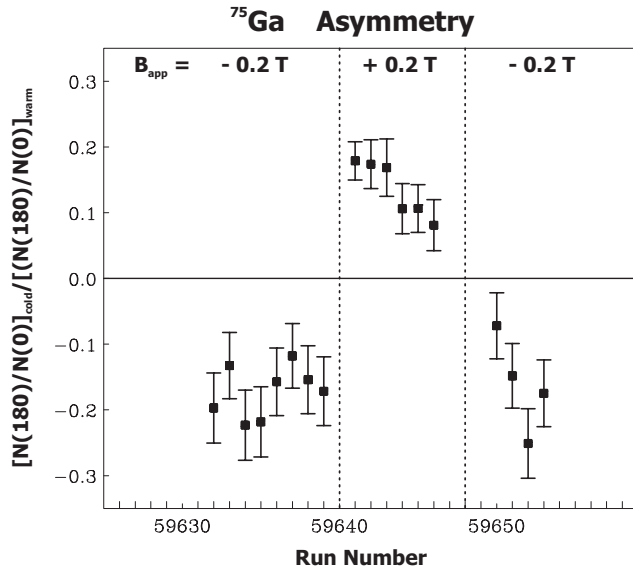

Fig. 49. Change in asymmetry as a function of applied magnetic field for β particles emitted from ^{75}Ga.
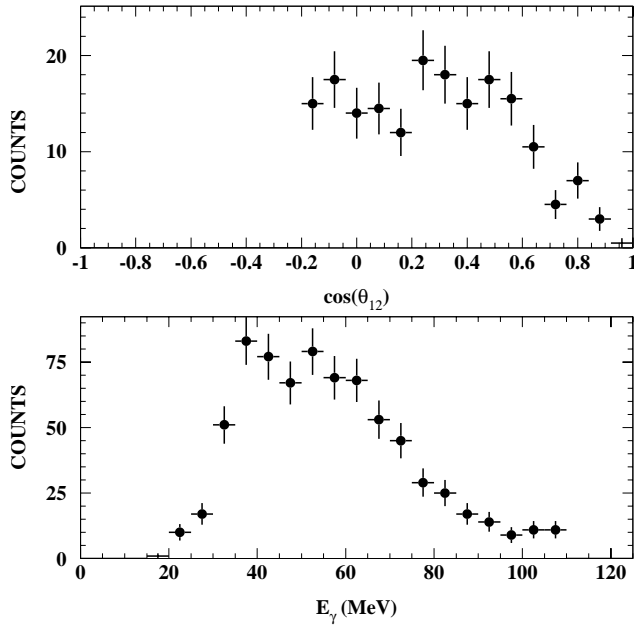
Fig. 50. The measured photon opening angle (top) and individual energy (bottom) spectra from double radiative capture on pionic deuterium.

drift chamber. An axial magnetic field was employed for momentum analysis and concentric plastic scintillator rings were employed for fast triggering.

The measured photon opening angle and individual energy spectra of the 386 recorded two-photon events from pionic deuterium are shown in Fig. 50. These spectra are entirely consistent with non-resonant double radiative capture. The expected signature of dibaryon events, i.e. a monoenergic peak from the production process $\pi^- d \to \gamma d^*$ and a three-body continuum from the decay process $d^* \to \gamma nn$, is not seen.

After correcting for the number of pion stops and the acceptance of the RMC detector we obtained a branching ratio upper limit on d^* production in $\pi^- d$ capture of $BR < 1.5 \times 10^{-6}$ (90% C.L.) for d^* masses of 1920–1980 MeV and d^* widths of <10 MeV. In particular we observed no evidence for a dibaryon of mass 1956 MeV and narrow width as claimed by Khrykin *et al.* Our upper limit on dibaryon production is several orders of magnitude below the yield estimate of Gerasimov.

Experiment 875
MuScat: muon scattering in low Z materials for muon cooling studies
(R. Edgecock, RAL; K. Nagamine, RIKEN)

As explained in the 2000 Annual Report, MuScat is making a precise measurement of the multiple scattering of muons in the momentum range 150–200 MeV/c. This measurement is of great importance to studies of ionization cooling, the process proposed for cooling muons for both a neutrino factory and a muon

collider [MUCOOL Collab., Fermilab Proposal P904 (1998)]. Due to the complexity of the cooling process and the fact that ionization cooling has never been demonstrated to work, MuScat is only the first of potentially three cooling experiments. The second of these is likely to be an upgrade of MuScat to measure the other physics processes of ionization cooling. This could form the subject of another proposal to TRIUMF. The last, the international muon ionization cooling experiment (MICE), will be a test of a prototype of the cooling channel for a neutrino factory. This will be a major experiment. The cooling section is likely to consist of eight 200 MHz rf cavities, eight superconducting solenoids and three liquid hydrogen absorbers each about 400 mm thick and 300 mm in diameter. This will be surrounded by two instrumentation sections, consisting of scintillating fibres similar to those to be used for MuScat (see below) contained in superconducting solenoids. There will also be time-of-flight counters and an electron identifier which could be very similar to the TINA calorimeter.

The layout of MuScat during the 2000 run is shown in Fig. 51. The most upstream parts were a veto shield and veto scintillator to eliminate beam halo. These were followed by the first trigger counter, which also acted as the TOF start. This is built from two fingers of scintillator, each 1 mm thick, 28 mm long and 3 mm high. These overlap by 20 mm in length and 3 mm in height. The timing resolution is about 250 ps. The TOF stop came from the following rf bucket of the cyclotron. This is almost a square-wave of length 1.9 ns, the smearing of the edges corresponding to a resolution of about 500 ps.

This trigger scintillator was followed by a 1 m long vacuum tube containing the collimation system. This consisted of a 40 mm thick lead block at the front and a 160 mm lead block at the back, plus 4 intermediate blocks each 10 mm thick. The first block had a slit 20 mm long by 2 mm high cut in it, while the slot in the second block was tapered to prevent large angle scatters off the internal face. With this arrangement,
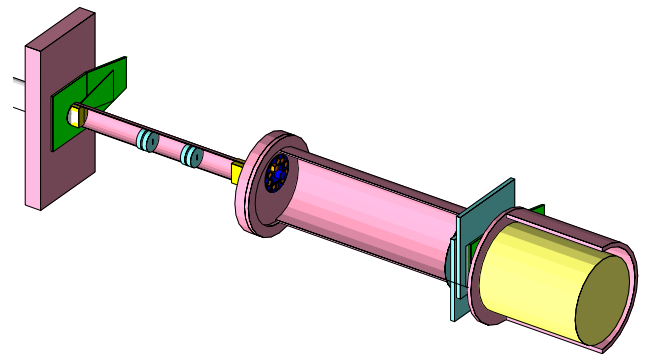

Fig. 51. The layout of the MuScat experiment in 2000, shown from below.

the scattering distribution was measured vertically, in the narrow direction of the slot. The second dimension was longer to increase the particle intensity.

The vacuum tube was connected to the main vacuum vessel, which contained the solid targets. In 2000, lithium, beryllium, carbon, aluminum and iron targets were used. They were mounted on a target wheel that could be controlled from outside the vacuum so it was unnecessary to break this each time a target was changed. The wheel had ten slots, the last of which had no target mounted and was used to measure the intrinsic properties of the beam.

The tracking detectors used were delay-line chambers. These are multi-wire proportional chambers with two cathode planes and one anode plane. Each chamber gives 2-dimensional readout, but with better resolution from the cathode plane perpendicular to the anode plane, ~ 0.6 mm compared to 1–2 mm. Rather than each wire being readout, the number of electronics channels required is reduced by recording only two signals from each plane. These are time values, giving the position along the delay-line from which the signal originated. As shown in Fig. 51, three of these chambers were used, each 300 mm by 300 mm in size. The most important of these was the first, which was orientated such that the dimension with the better resolution was vertical. It was approximately 1 m from the target wheel. Between the second and third chambers was the second trigger scintillator.

The final part of the detector was MINA, a NaI calorimeter of 360 mm diameter and 360 mm depth [Waltham *et al.*, Nucl. Instrum. Methods **A256**, 91 (1987)]. It has a measured energy resolution (fwhm) of 5.2% at 90 MeV with an energy dependence of $E^{-0.55}$. It was used for both a muon energy measurement and additional pion/muon separation.

During 2001, a number of improvements were made for a second run in 2002, based on the experience gained in 2000. These improvements are described in the following sections.

Detectors

The delay-line chambers used for the first run of MuScat were found to have a rapid and non-uniform loss in efficiency during the running period (see the 2000 Annual Report). As a result, it was decided to replace these with three new chambers built from scintillating fibres. These consist of two offset planes of 1 mm thick fibres in each dimension, to give a uniform efficiency and two dimensional readout. Two of the chambers, which are 30 cm by 30 cm, are shown under construction in Fig. 52. There is a total of 1024 fibres per chamber. Unlike the delay-line chambers, they will be mounted inside the vacuum to remove all material between them and the targets.
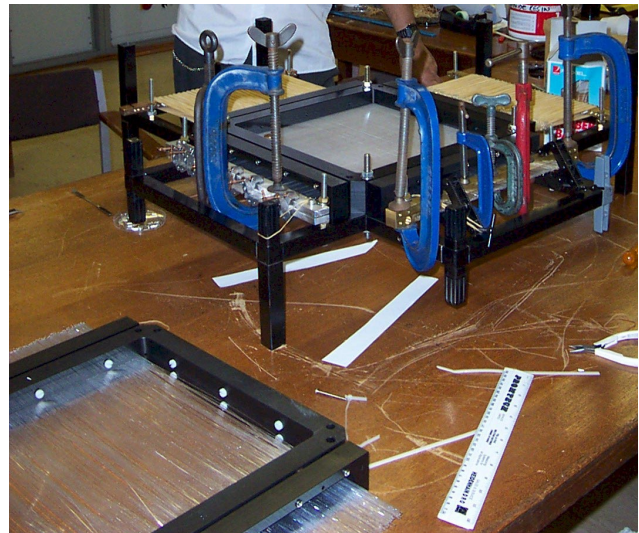

Fig. 52. Two new scintillating fibre detectors shown under construction at Imperial College, London.

The light from the scintillating fibres is transmitted to photomultipliers using clear fibres. The PMTs used are Hamamatsu R5900 L16s (see http://cat1.hpk.co.jp/Eng/catalog/ETC/R5900U-L16_TPMH1146E06.pdf) and contain 16 anodes, each 16 mm long and 0.8 mm wide. An array of 16 by 16 clear fibres is formed to match these anodes, thus giving a 16-fold multiplexing. To ensure that signals can be de-convoluted, the scintillating fibres are read out at both ends and the PMTs at each end are rotated by 90° with respect to each other. The PMTs sit outside the vacuum vessel and the fibre arrays form the vacuum seal. Tests show that the leak rate from these is sufficiently small to allow a vacuum of less than 10^{-6} torr.

Purpose built front-end sample and hold electronics are used to readout the PMTs. The analogue signals from this are digitized using an ADC mounted on a card in one of the DAQ computers.

At year end, all the chambers and the 24 clear fibre arrays have been built. These are currently being inserted into the connectors that match them to the scintillating fibres. All the readout electronics are also complete. One chamber has been tested in an accelerator beam. Figure 53 shows the signals from this chamber, converted into the number of photoelectrons seen. A cosmic ray rig is being built to continue the chamber testing.

Collimation system

The performance of the collimation system in 2000 is shown in Fig. 54, with a number of software cuts applied, including tracking back to the target region, to minimize background. Although this is adequate for the aims of MuScat, it was decided to reduce both the
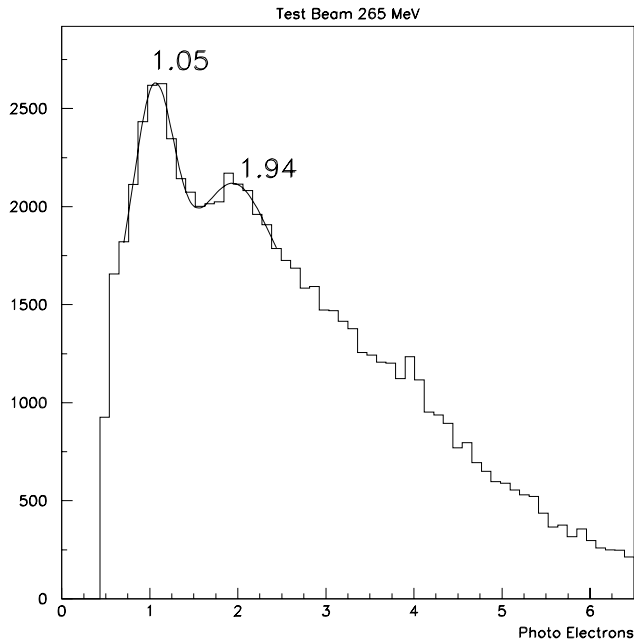
Fig. 53. Signals from a scintillating fibre detector using a 265 MeV/c mainly pion beam. A calibration has been applied which is believed to convert the signal into photoelectrons. Fits made indicate that the first two peaks do correspond to one and two photoelectrons, respectively.
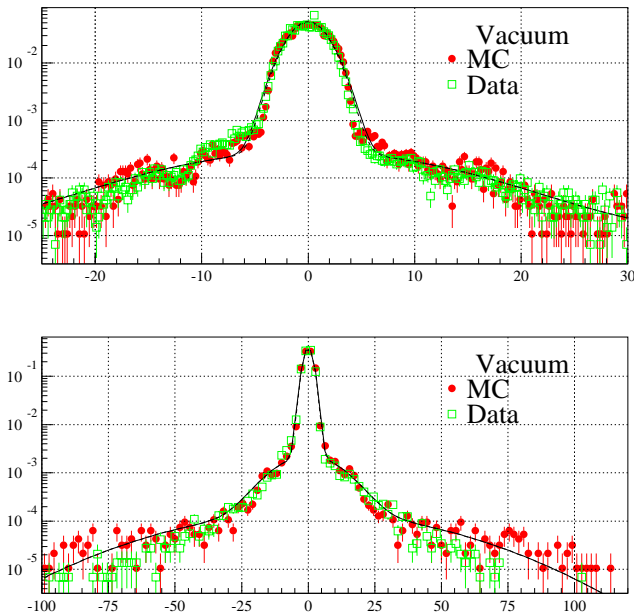

Fig. 54. The distribution of hits in the most upstream delay-line chamber without a target. The open squares are data from 2000 and the closed circles are MC predictions. The lines are the result of the fit of three Gaussians. The bottom plot shows the hits from ± 100 mm, while the top is zoomed to –25 to +30 mm.

width of the peak and the size of the tails of the no target scattering distribution for 2002. This has been done by moving the existing collimator disks in the collimator tube to the ends, two to each, to increase the
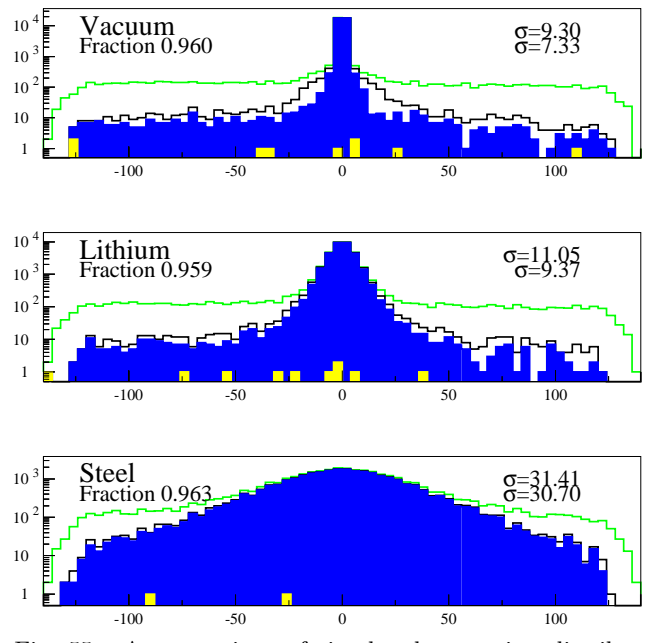

Fig. 55. A comparison of simulated scattering distributions with no target, 10 mm of lithium and 2 mm of iron using the old and new collimation systems. In each case, the upper line is the old collimation system, with no software cuts, the middle line is the new system and the dark shaded area is the new system using the active collimator. The light shaded blocks are from decays in flight.

thickness of the 40 mm and 160 mm thick end collimators. The disks have been replaced by another four, each 10 mm thick, but with 2 cm radius holes through the centre. As well as reducing the penetration through the collimators, this dramatically reduces large angle scatters off the internal faces of all the collimators. The large angle scatters will be further reduced by wrapping the collimator tube with 6 mm thick lead sheet and doubling the thickness of the front flange of the main vacuum vessel. Finally, an active collimator is being added to the front face of the 160 mm collimator block. This is being done by placing small blocks of scintillator above and below the slit of the collimator. This will eliminate particles that just clip this edge of the collimator. These improvements are demonstrated in Fig. 55.

Targets

In the 2000 run, nine different solid targets were used, mounted on the ten hole target wheel. The tenth hole was used for measuring the intrinsic distribution of the beam. For the run in 2002, a twelve hole wheel has been created. This will allow nine targets of the same type as in 2000 to be used, but thicker to allow for the use of a higher beam energy than originally expected. In addition, one target from 2000 will be re-used, to have a comparison with the previous data. Finally, it is hoped to use a lithium hydride target, if a solid piece of the required size can be obtained.

However, the main change compared to 2000 will be two liquid hydrogen targets, one 100 mm thick and the other 150 mm. These have been built by the Cryogenics group at TRIUMF. Two thicknesses are to be measured to make it easier to de-convolute the effects of the target windows.

Vacuum vessel

Due to the new scintillating fibre detectors and the liquid hydrogen targets, a new main vacuum vessel has been built. This vessel has a large port for the LH2 targets and larger diameter section at the end for mounting the three detectors and providing ports for the clear fibre bundles to be connected to the PMTs. In addition, there is an expansion length to be inserted when the LH2 targets are used to maintain the same distance between the middle of these and the solid targets. The vessel has been tested to the vacuum level required for the LH2 targets and pressure tested to the required safety standards.

In addition, a new stand has been built to hold the new vacuum vessel. This has also been made long and strong enough to support MINA. The mounting mechanism has been improved to allow easier alignment of the experiment.

The final change to the experiment is a larger trigger scintillator at the back of the experiment to cover the full active area of the detectors.

Experiment 879
^{21}Na(p, p) resonant elastic scattering
(C. Ruiz, Edinburgh)

This experiment used a newly available radioactive ^{21}Na beam at TRIUMF's ISAC facility to study the resonant elastic scattering of ^{21}Na on protons, with the intention of determining states in the compound nucleus system ^{22}Mg.

^{21}Na $(T_{1/2} = 22.49$ s) beams of energies between 0.5 and 1.56 MeV/nucleon were accelerated through the ISAC-DTL and transported via the HEBT line to the TUDA particle scattering facility (TUDA collaboration: TRIUMF, University of Edinburgh, University of York). Here, highly segmented axially-symmetric LEDA silicon detector arrays were used to detect the recoil protons scattered from various thicknesses of CH$_2$ targets. The energy loss of the incident ^{21}Na through the thick CH$_2$ targets (between 250 μg/cm^2 and 50 μg/cm^2) enabled the detection of protons from a range of centre-of-mass scattering energies. Therefore a range of corresponding excitation energies in the compound nucleus system can be studied.

The maximum ^{21}Na beam intensities achieved were of the order 5×10^8 particles/s, however, data aquisition constraints forced the use of a lower intensity

during the main experiment. The intensities used (typically 5×10^7 particles/s) enabled the collection of spectra with high statistics over a short period of time. Three broad s-wave resonances in the centre-of-mass region between 0.7 and 1.5 MeV were identified, and an ongoing analysis of the data may yet reveal more. The data obtained will provide useful information on the T=1, A=22 mirror system, and may also contribute to the detailed understanding of the astrophysically important ^{21}Na$(p, \gamma)^{22}$Mg reaction.

The experimental set-up

The TUDA facility was designed as an all-purpose particle scattering facility, providing up to 512 channels of particle detection, and a range of possible target types and positions. TUDA is particularly suited to resonant elastic scattering experiments due to the highly segmented nature of the detectors, enabling detection of recoil protons over a range of different centre-of-mass angles with high statistics. Not only can excitation functions be determined over the centre-of-mass energy range, but angular distributions can be determined providing vital information on the spin and parity of the resonant states.

In this experiment, two LEDA detectors were used at 20 cm and 62.8 cm from the target position, covering lab angles of 4.552°–11.687° and 14.036°–33.004° respectively. These correspond to a centre-of-mass energy range of approximately 156.6°–170.9° and 114.0°–151.9°, enough to determine angular distributions for strong p-waves, for example. Each LEDA detector comprises eight azimuthal sectors with sixteen annular strips at different angles.

Both LEDA detectors were shielded with a thin mylar film to prevent the scattered ^{21}Na and recoil ^{12}C
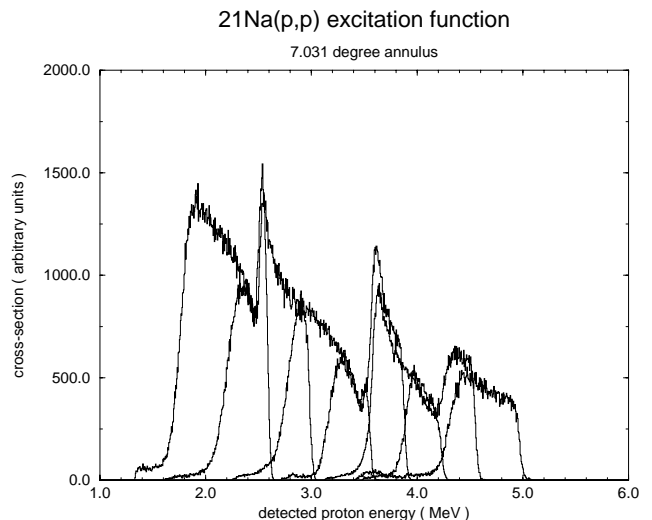

Fig. 56. Thick target proton spectra at beam energies of 880, 990, 1144, 1240, 1340, 1440 and 1560 keV/nucleon, for one annulus of a LEDA detector.

from the CH_2 targets from hitting the silicon. One of the eight azimuthal sectors was left uncovered by the mylar, and its corresponding electronics set at a lower gain to allow the collection of eight heavy-ion spectra for the purpose of normalization.

The centre-of-mass energy scan for a 250 $\mu g/cm^2$ target is approximately 200 keV. Thus, beam energies were chosen so that each thick target run would overlap substantially with the previous one, enabling target edge effects to be rejected in the final excitation function. An example of the overlapping thick target spectra for one angle can be seen in Fig. 56.

Data reduction and preliminary results

The data were normalized by the beam via the detected ^{21}Na in the low gain sector. The cross section was evaluated over the angular range of each strip and the energy range of the thick target to provide an accurate estimate of the number of incident ^{21}Na ions. The data were also normalized to the amount of hydrogen in the CH_2 targets, which tends to deplete over time exposed to the beam, by a similar method involving the proton spectra obtained in the low gain sector. The normalization factors were then applied to each thick target spectrum, and the edges of each spectrum cut off to exclude target edge effects. The resulting data were concatenated, examples of which can be seen in Fig. 57.

Elastic scattering of ^{21}Ne$+p$ was also performed over several known resonances for the purpose of energy calibration of the ^{21}Na data. This will be combined with a calibration from the target edges using the known beam energies.

In Fig. 57, the two spectra at largest angles show a discontinuity in the excitation functions caused by different thicknesses of mylar used for the different beam energies on the LEDA detector at 20 cm. Also, the straggling of the protons in the thick target and mylar, combined with the kinematic spread due to the
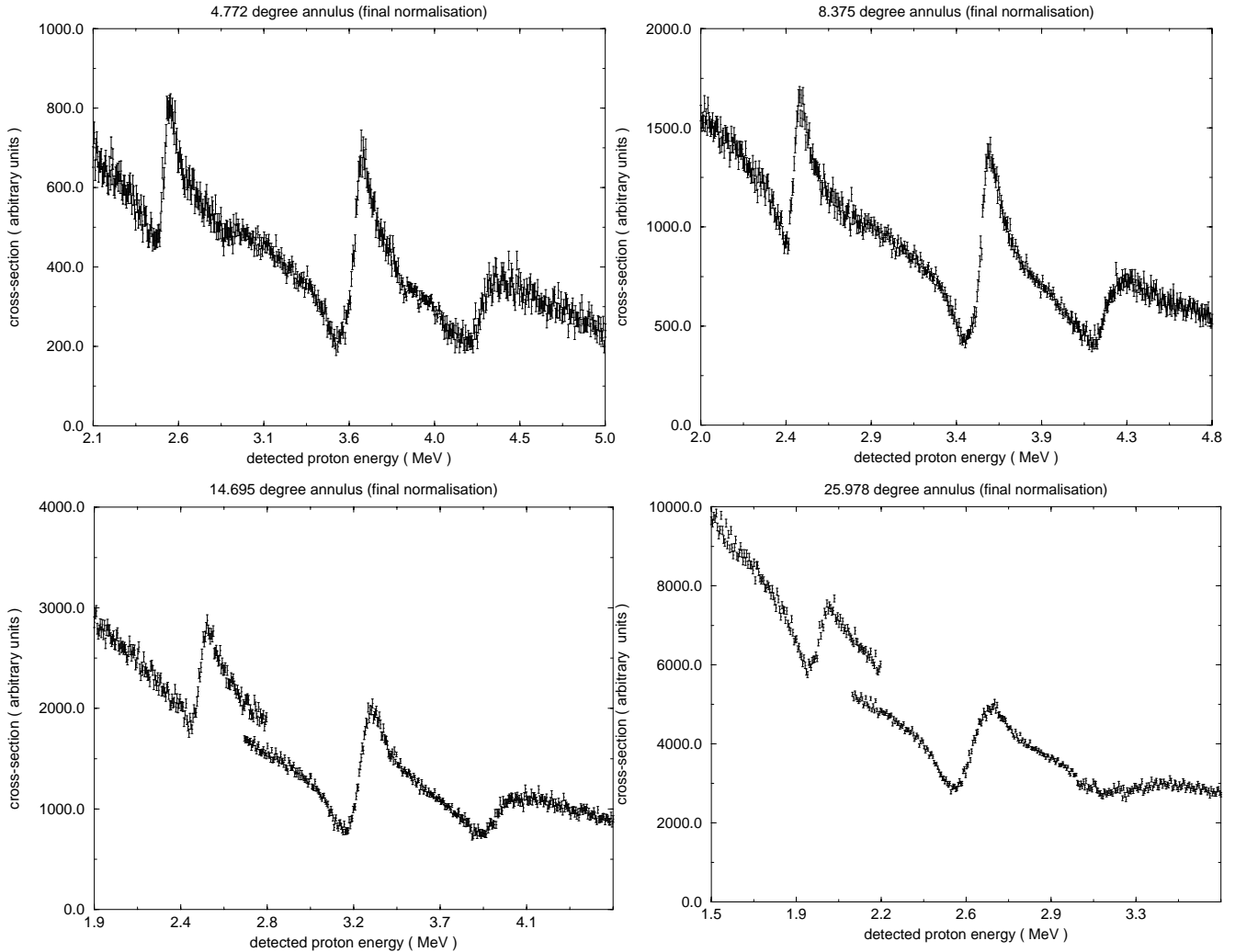

Fig. 57. ^{21}Na$+p$ excitation functions for a selection of the 32 separate angles.

angular opening of each detector strip, causes the excitation function to be convoluted, as can be seen from the higher angle spectra. At present a Monte Carlo simulation is under construction to determine the size and type of convolution required for a fit to these spectra.

An R-matrix fit for all angles is required to determine accurately the widths and resonance energies of the observed states. A preliminary R-matrix fit for the smallest angle data has been performed and the results have been submitted for publication.

Concluding remarks

The first radioactive beam experiment performed at ISAC using the TUDA particle scattering facility has been succesfully completed, and an ongoing data analysis is under way. Preliminary results have been submitted for publication. It is expected that the final results will have been submitted for full publication by the end of 2002. The analysis of the data will form the major part of the thesis of C. Ruiz, University of Edinburgh.